Supplementary information

for

Sulfophenylated centimeter-size graphene membrane in a direct methanol fuel cell

Weizhe Zhang[1]*, Max Makurat[1], Xue Liu[1,2], Buhang Chen[3,4], Yanglizhi Li[3,4], Xiaoting Liu[3,4], Thomas J.F. Kock[1], Andy Jiao[1], Guangya Jiang[1], Christopher Leist[5], Clément Maheu[6,7], Hikmet Sezen[6], Dario Calvani[1,8,9], Ismail Eren[10], Lin Jiang[1], Francesco Buda[1], Haoyuan Qi[5], Jan P. Hofmann[6], Xinliang Feng[11,12], Ute Kaiser[5], Luzhao Sun[3,4], Zhongfan Liu[3,4],Agnieszka Kuc[8,9], Thomas Heine[8,9,13,14], Grégory F. Schneider[1]*

[1] *Leiden Institute of Chemistry, Faculty of Science, Leiden University, Einsteinweg 55, 2333CC Leiden, The Netherlands.*

[2] *State Key Laboratory for Mechanical Behavior of Materials, Xi'an Jiaotong University, 710049 Xi'an, China.*

[3] *Beijing Graphene Institute (BGI), Beijing, China.*

[4] *Center for Nanochemistry, Beijing Science and Engineering Center for Nanocarbons, Beijing National Laboratory for Molecular Sciences, College of Chemistry and Molecular Engineering, Academy for Advanced Interdisciplinary Studies, Peking University, Beijing, China.*

[5] *Central Facility of Electron Microscopy, Electron Microscopy Group of Materials Science, Ulm University, Ulm, Germany.*

[6] *Surface Science Laboratory, Department of Materials and Earth Sciences, Technical University of Darmstadt, Peter-Grünberg-Straße 4, 64287 Darmstadt, Germany.*

[7] *Université de Nantes, CNRS, Institut des Matériaux de Nantes Jean Rouxel, IMN, F-44000 Nantes, France*

[8] *Center for Advanced Systems Understanding (CASUS), Untermarkt 20, 02826 Görlitz, Germany*

[9] *Helmholtz-Zentrum Dresden, Rossendorf (HZDR), Bautzner Landstr. 400, 01328 Dresden, Germany*

[10] *Helmholtz-Zentrum Dresden-Rossendorf, Abteilung Ressourcenökologie, Permoserstrasse 15, 04318 Leipzig, Germany.*

[11] *Center for Advancing Electronics Dresden & Faculty of Chemistry and Food Chemistry, Technische Universität Dresden, Dresden, Germany.*

[12] *Max Planck Institute of Microstructure Physics, 06120 Halle (Saale), Germany.*

[13] *Theoretical Chemistry, Technical University Dresden, 01062 Dresden, Germany.*

[14] *Yonsei University and ibs-cnm, Seodaemun-gu, Seoul 120-749, Republic of Korea*

* to whom correspondence should be addressed: w.zhang@lic.leidenuniv.nl, g.f.schneider@chem.leidenuniv.nl

This PDF file includes:

and

Figures S1 to S33 and Tables S1 to S4.

1. Theoretical study on proton transport through functionalized graphene.

1.1 Tunneling Calculations.

We modeled graphene using circumcoronene, which was subsequently functionalized with various groups (H, phenyl, protonated and deprotonated sulfophenyl). Always, two neighboring carbon atoms were functionalized to prevent radical formation, with the groups positioned on opposite sides of the circumcoronene ring. Systems were fully optimized using the PBE0 hybrid density functional, TZP basis set, many-body dispersion (MBD) correction, and good numerical quality settings, as implemented in the AMS suite[1,2]. Once optimized, we substituted functional groups with H atoms (Fig. S1) and investigated hexagonal ring distortion's impact on proton tunneling through the rings. The potential energy barriers were determined through DFT calculations using the Born-Oppenheimer approximation (as described above), while corresponding particle fluxes through the membrane were calculated using the Wentzel–Kramers–Brillouin (WKB) approximation, as described in our previous work[3].

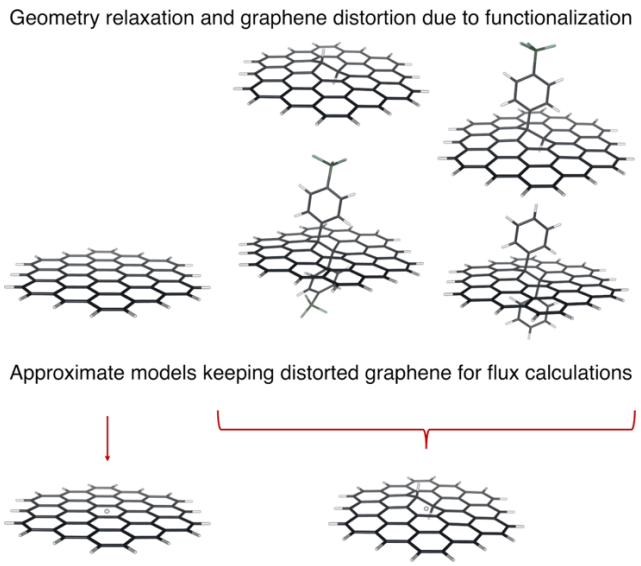

Fig. S1. Simulations models: Step 1, all models were relaxed as explained in the Methods section; **Step 2,** all the functional groups were substituted by H atom at their

relaxed geometries; **Step 3,** new models were used to obtain DFT potential energy barrier, to be used in **Step 4,** to calculate the proton flux employing WKB approximation.

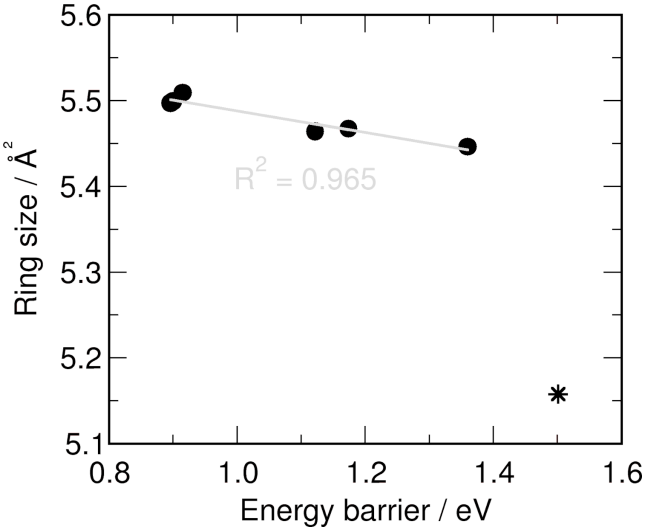

Fig. S2. Correlation between ring area and the energy barrier for proton transfer through graphene (using circumcoronene model structure). Energy barrier calculated at the DFT/PBE0/MDB level of theory; ring area calculated via triangle area summation in a 6-fold ring. Pristine graphene is marked with a star, the functionalized graphene with black circles. For the set of points for functionalized graphene, we find a linear correlation between the ring area and the energy barrier.

Table S1 Flux of proton calculated at 300 K using WKB approximation.

System	Ring area (Å^2)	Classical flux	Quantum flux	Total flux
graphene	5.158	1.738×10^{-29}	5.994×10^{-27}	6.011×10^{-27}
2H graphene	5.446	4.405×10^{-27}	2.165×10^{-26}	2.606×10^{-26}
SBD-graphene	5.464	9.073×10^{-23}	3.978×10^{-22}	4.886×10^{-22}
protonated SBD-graphene	5.467	5.358×10^{-24}	3.595×10^{-23}	4.131×10^{-23}
2-side SBD-graphene	5.497	2.832×10^{-19}	9.996×10^{-19}	1.283×10^{-18}
protonated 2-side SBD-graphene	5.509	1.304×10^{-19}	4.712×10^{-19}	6.016×10^{-19}

2-side phenyl-graphene	5.499	2.227×10^{-19}	7.802×10^{-19}	1.003×10^{-18}

The particle flows (flux) are given in hartree atomic units of length/time.

1.2 ReaxFF-MD simulations.

The ReaxFF-MD simulations[4-6] are performed using the AMS2021 suite[7,8] and the CHONSMgPNaTiClFKLi.ff force field[9-11] suitable for describing these systems in a water environment[12]. We build up the starting system from a 17.22 Å × 17.04 Å graphene layer placed in a cell of 17.22 Å × 17.04 Å × 25.00 Å dimension (Fig. S3). A sulfophenylated sp^3 functionalization is added to the graphene basal plane. The system is solvated with 170 water molecules to reach a density of ~ 1.0 g mL^{-1}. Periodic Boundary Conditions (PBC) are applied. ReaxFF-MD equilibrations are performed for 0.5 ns each, with a time step of 0.25 fs and a damping constant of 1000 and 100 for pressure and temperature, respectively. First, an NPT equilibration run is performed at 300 K and 1 atm using the Martyna-Tobias-Klein (MTK) barostat and the Nosé-Hoover chains (NHC) thermostat. Secondly, the system is further equilibrated in the NVT ensemble with the NHC thermostat at 300 K. The dimension of the simulation cell for the NPT equilibration is kept constant along x- and y-the axis (17.22 Å × 17.04 Å parallel to the graphene sheet) and changes only along the z-axis to 24.23 Å. The total charge is -1. After adding a proton to the system in the water bulk, the total charge is equal to 0, and another 0.5 ns NVT equilibration is executed with the NHC thermostat at 300 K. Finally, the production run NVT ReaxFF-MD plus metadynamics[13,14] simulation of 1.0 ns is performed employing the PLUMED plugin[15] for the

metadynamics, NHC thermostat at 300 K. We employ a well-tempered metadynamics method with width = 0.5 Å, height = 0.1 kJ mol^{-1}, bias factor = 10, and deposition frequency of Gaussian hills every 100-time steps[16]. In Fig. S4, the obtained free energy profile and activation Gibbs free energy barrier are shown. Noteworthy, assuming negligible volume changes during simulations, the Gibbs free energy can be replaced with the Helmholtz free energy, described by the NVT ensemble.

The Collective Variable used for describing the proton traveling from the sulfophenylated sp^3 functionalization into the water bulk is defined as the distance from the center of mass of the oxygens of the sulfonic group (Ph-SO_3^-/Ph-SO_3H) to the oxygen atom of the hydronium ion/water molecule coordinated to the proton in the functional group[17].

$$L = f(n_G)\left[\frac{\sum_{i\in\{O_w\}} d_i exp\,(\lambda n_i)}{\sum_{i\in\{O_w\}} exp\,(\lambda n_i)}\right]$$

where $d_i = |r_i - r_G|$ is the distance between oxygen atom i and the center of mass of the oxygen atoms belonging to the functional group, and n_G is the hydrogen coordination number of the functional group. The switching function $f(n_G)$ included in the Collective Variable is given by:

$$f(n_G) = \frac{1 - \left(\frac{n_G}{n_c}\right)^6}{1 - \left(\frac{n_G}{n_c}\right)^{12}}$$

where the coordination cutoff n_c is a parameter whose value depends on how many excess protons are present in the system.

The switching function $f(n_G)$ is included in the Collective Variable since the distance calculated by the function in square braces would not be meaningful if the functional group is protonated. For instance, at the start of the ReaxFF-MD metadynamics simulation when the functional groups are protonated, the value of the Collective Variable is near zero since $n_G = 1$ $(f(n_G) \approx 0)$ and consequently, the Collective Variable is close to zero. The switching function $f(n_G) \approx 1$ resulting in Collective Variable depending on the value in square braces and describing the distance between the center of mass of the oxygens of the sulfonic group (Ph-SO_3^-/Ph-SO_3H) to the oxygen atom in the hydronium ion/water molecule coordinated to the proton in the functional group.

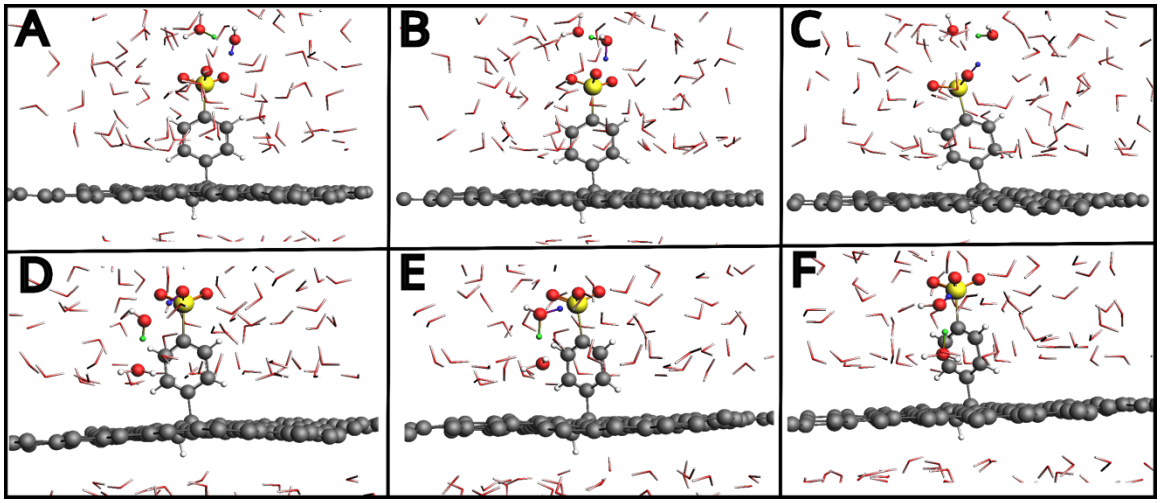

Fig. S3 Representative ball and stick snapshots of the sulfophenylated *sp*³ defect functionalization of graphene layer solvated in water at different steps of the

Grotthuss mechanism and proton shuttling towards the graphene basal plane. (**A**) Hydronium in the water bulk upper side of the simulation box; (**B**) proton hopped on the nearest water to the SO_3^- of the sulfophenylated sp^3 functionality; (**C, D**) proton captured and shuttled by the sulfophenylated functionality, respectively; (**E**) proton released above the SO_3^- of the sulfophenylated sp^3 functionality forming a hydronium; (**F**) proton hopped on a water closer to the basal plane (~3 Å) forming a hydronium. For clarity, sulfophenylated sp^3 defect functionalization of graphene and molecules in the proton network are represented by balls and sticks: carbon, oxygen, sulfur, hydrogen, and the protons involved in the Grotthuss Mechanism are colored in grey, red, yellow, white, blue and green, respectively. The rest of the water molecules are shown as sticks.

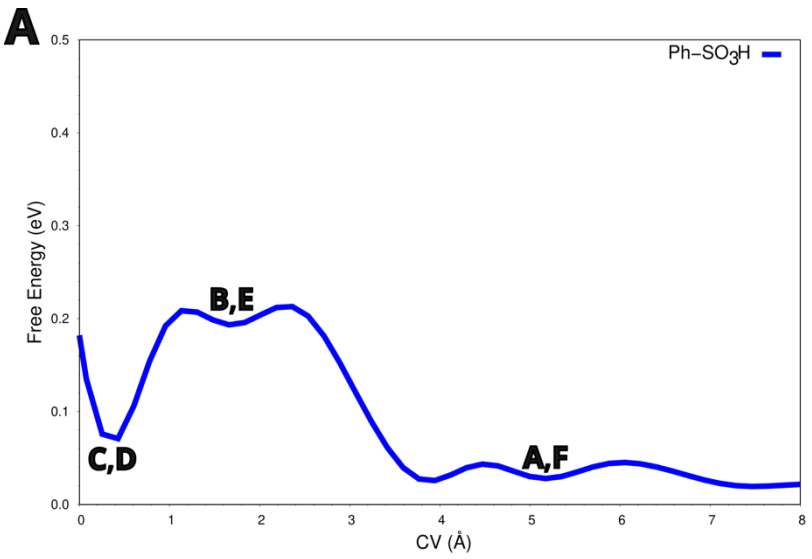
A
Ph–SO3H
Free Energy (eV)
B,E
C,D
A,F
CV (Å)

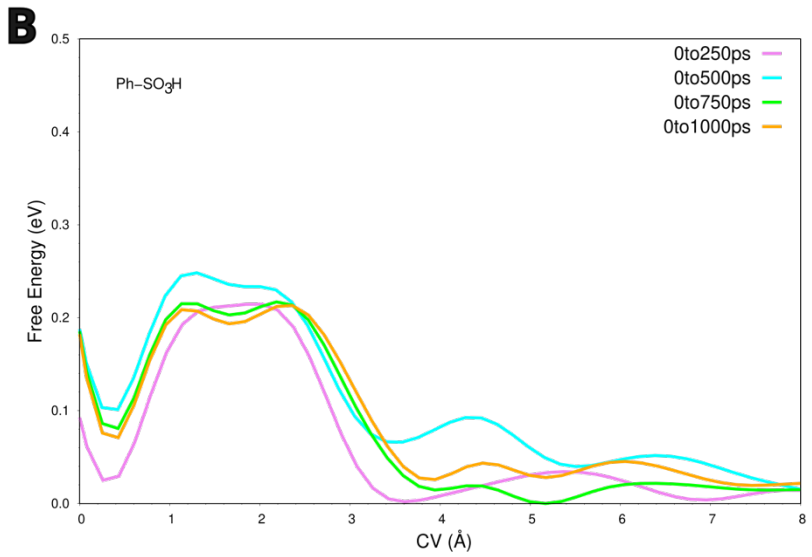
B
Ph–SO3H
0to250ps
0to500ps
0to750ps
0to1000ps
Free Energy (eV)
CV (Å)

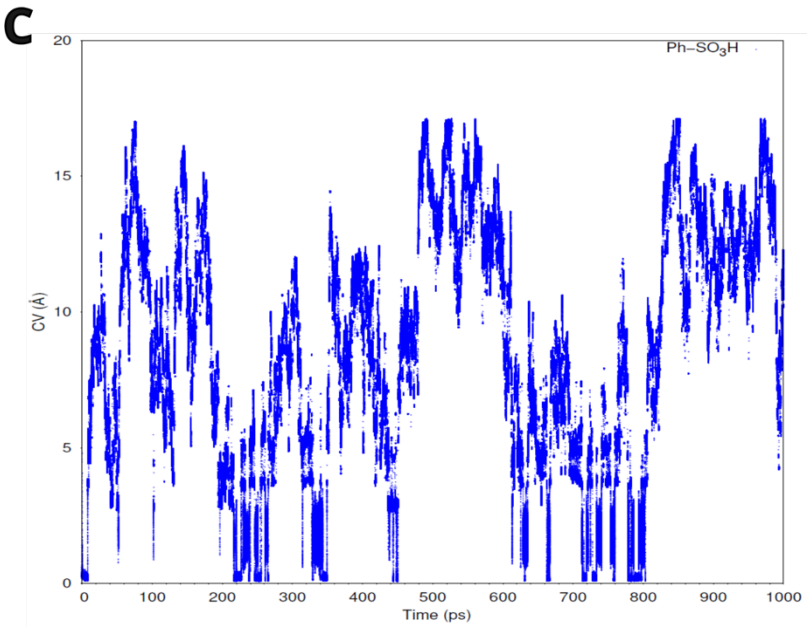
C
Ph–SO3H
CV (Å)
Time (ps)

Fig. S4 Free energy profile and time evolution of Collective Variable of the simulation for SO_3^--graphene. (**A**) Free energy profile (eV) along the Collective Variable CV (Å) over 1.0 ns of the simulation for graphene with sulfophenylated sp^3 defect functionalization, blue line. The inset capital letters connect the representative configurations in Fig. S3 to the Free Energy Surface regions. (**B**) Free energy convergence (eV) of the simulation for graphene with sulfophenylated sp^3 defect functionalization along CV (Å). To assess the convergence of a metadynamics simulations, each free energy profile is extracted after 0.25 ns (violet line), 0.5 ns (cyan line), 0.75 ns (green line), and 1.0 ns (orange line) of the simulation, with a deposition stride every 25 fs, and the global minimum is set to zero in all profiles. (**C**) Time evolution of the Collective Variable CV (Å) of the simulation for graphene with sulfophenylated sp^3 defect functionalization.

2. Single-crystalline CVD graphene before and after 4-SBD treatment.

2.1 4-sulfonato-benzene-diazonium (4-SBD) synthesis.

All solvents and reagents were obtained from commercial sources (Sigma Aldrich and Merck) and used without further purification unless stated otherwise in the respective method section. ^{1}H, ^{13}C, and ^{19}F NMR spectra were recorded on a Bruker AV 400 MHz spectrometer and the chemical shifts are reported in ppm (δ) with respect to deuterated solvents as an internal standard. The data is reported as chemical shift (δ), multiplicity (d = doublet), and coupling constants *J* are reported in Hz. High-resolution mass spectra

were recorded by direct injection (2 µL of a 2 µM solution in water/acetonitrile; 1:1 v/v with 0.1 % formic acid) on a Q-Exactive HF Orbitrap (Thermo Scientific) equipped with an electrospray ion source (source voltage 3.5 kV, 275 °C capillary temperature and no sheath gas) via Ultimate 3000 nano UPLC (Dionex) system, with an external calibration (Thermo Scientific). The resolution was 240.000 at m/z = 400 and the mass range was m/z = 160-2000.

To prepare 4-SBD in salt form with tetrafluoroborate as counterion, a suspension of sulfanilic acid (2.00 g, 11.5 mmol, 1.0 eq) in 48% aqueous tetrafluoroboric acid (4 mL, 30.3 mmol, 2.6 eq) was cooled to -5 °C. While stirring a pre-cooled aqueous saturated solution of sodium nitrite (1.20 g, 17.3 mmol, 1.5 eq) was added dropwise to the reaction mixture. During the addition, it became increasingly difficult to maintain stirring which was solved by adding 4 mL of cooled ultrapure water. After this, the reaction mixture was stirred at -5 °C for 5 h after which the product was isolated by filtration. The collected precipitate was washed with ice-cold diethyl ether, ice-cold diethyl ether/methanol (4:1 v/v), ice-cold ethanol and dried overnight under vacuum to yield 4-SBD as a white solid (2.43 g, 9.94 mmol, 77 %). The compound was stored at 4 °C. ^{1}H NMR (400 MHz, DCl 0.1 M/DMSO-d_6) δ 8.63 (d, J = 8 Hz, 2H), 8.18 (d, J = 8 Hz, 2H). ^{13}C NMR (100 MHz, DCl 0.1 M/DMSO-d_6) δ 156.7, 134.8, 130.2, 118.5. ^{19}F NMR (376 MHz, DCl 0.1 M) δ -150.6. ESI-HRMS (m/z): $C_6H_5N_2O_3S^+$ [M+] calculated: 185.00, found: 185.00. For all experiments 4-SBD was prepared fresh or used within a timeframe of two months while being stored at 4 °C between experiments.

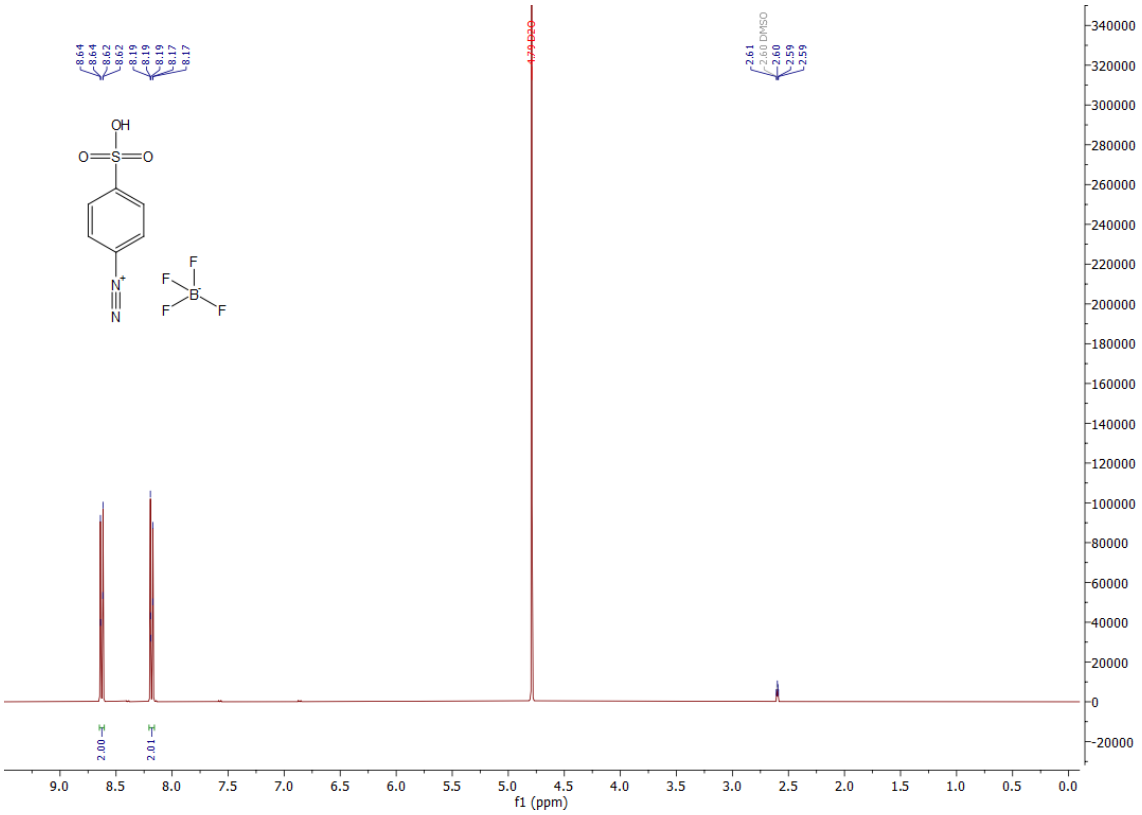

Fig. S5 ^{1}H NMR spectrum of 4-SBD.

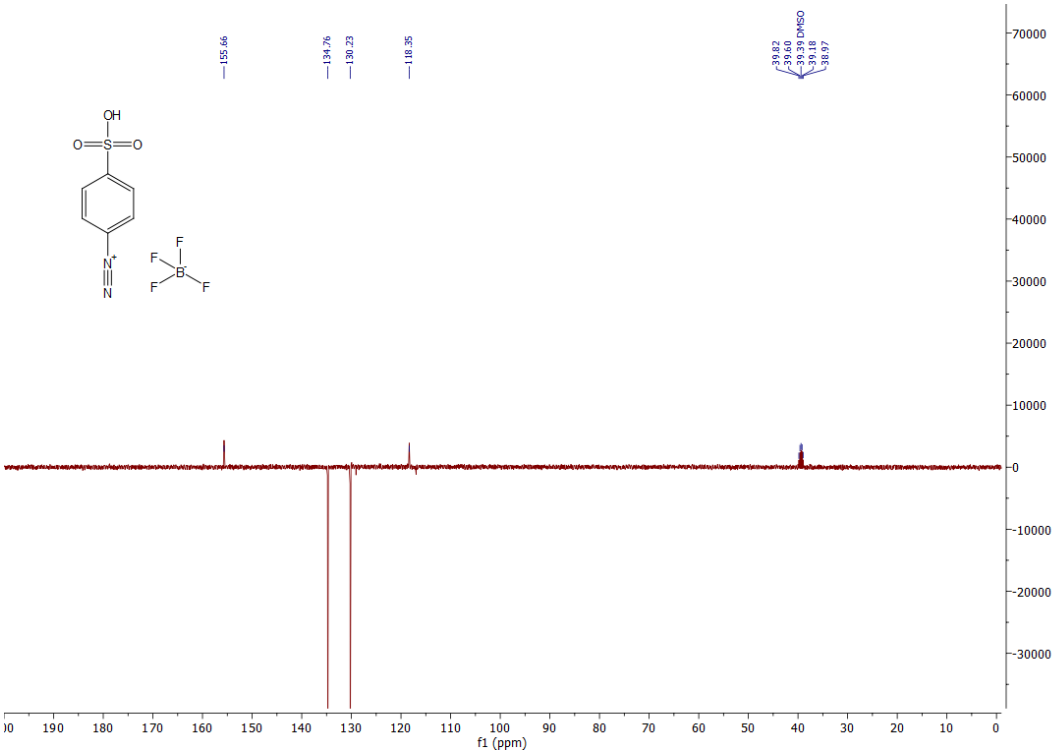

Fig. S6 ^{13}C-APT spectrum of 4-SBD.

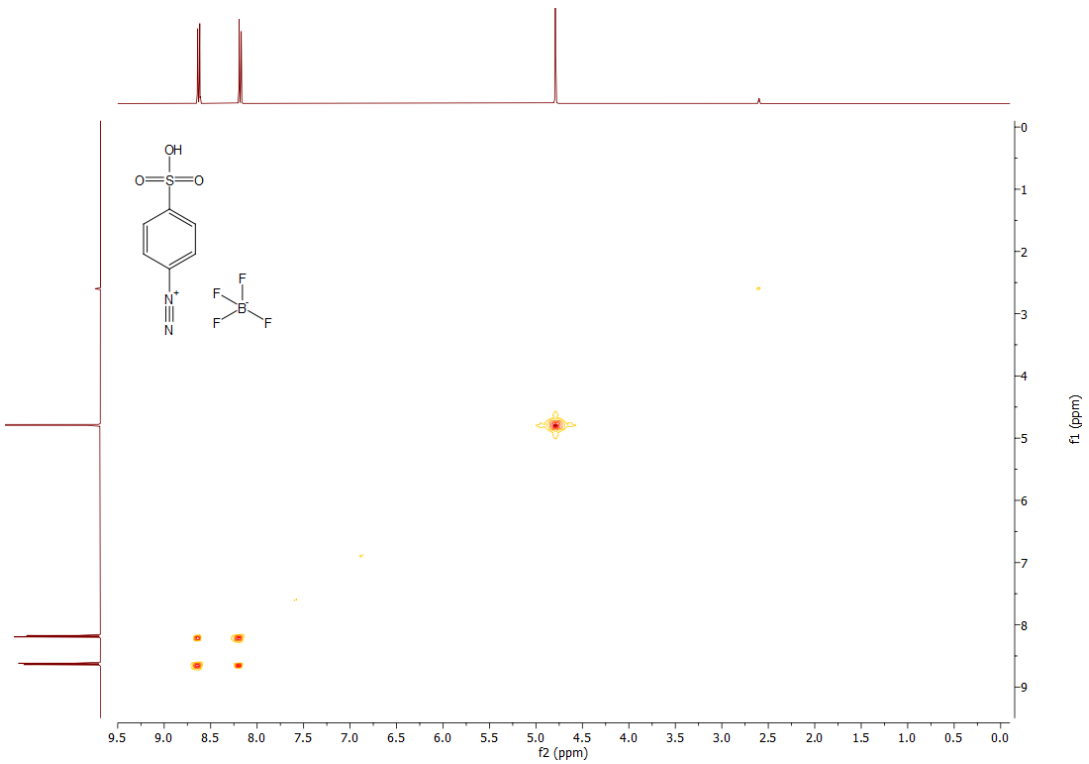

Fig. S7 COSY spectrum of 4-SBD.

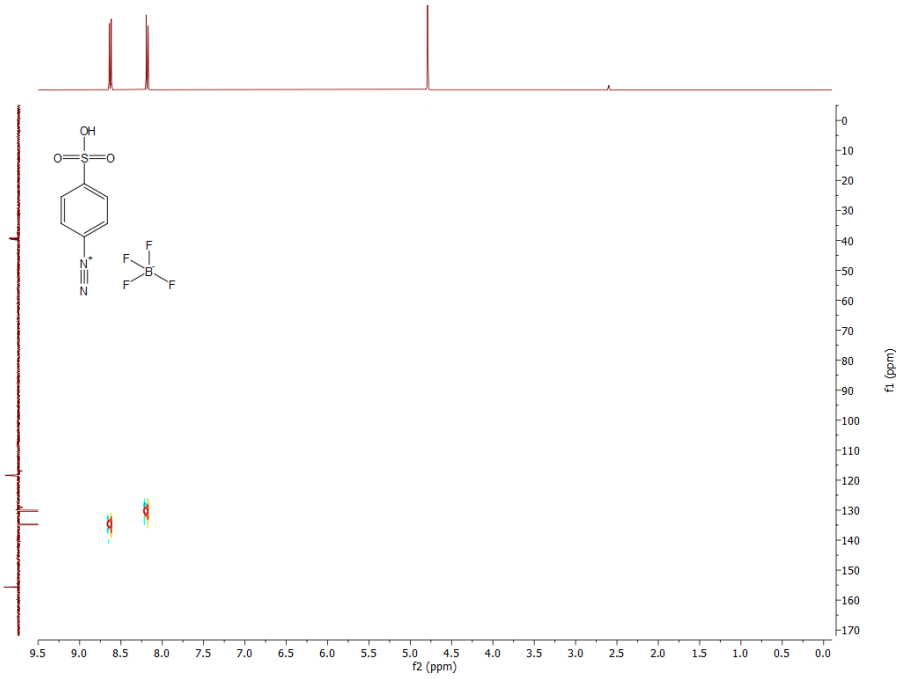

Fig. S8 HSQC spectrum of 4-SBD.

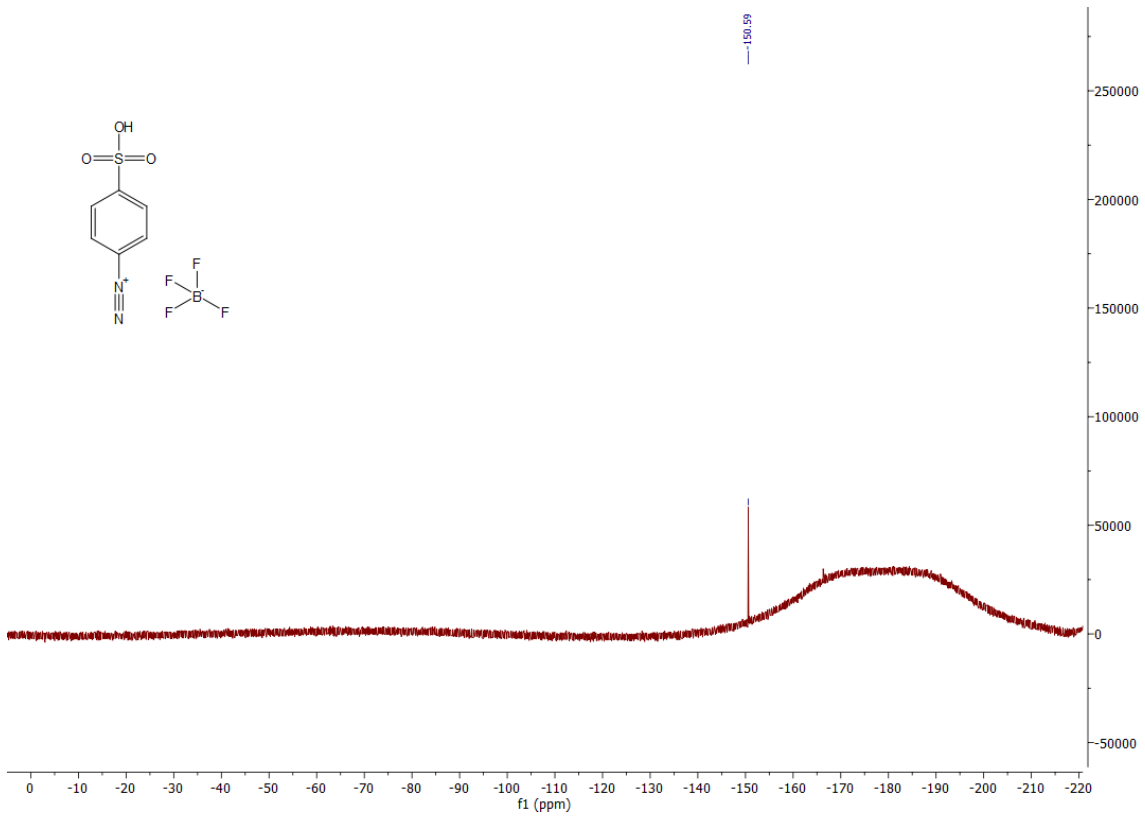

Fig. S9 ^{19}F NMR spectrum of 4-SBD.

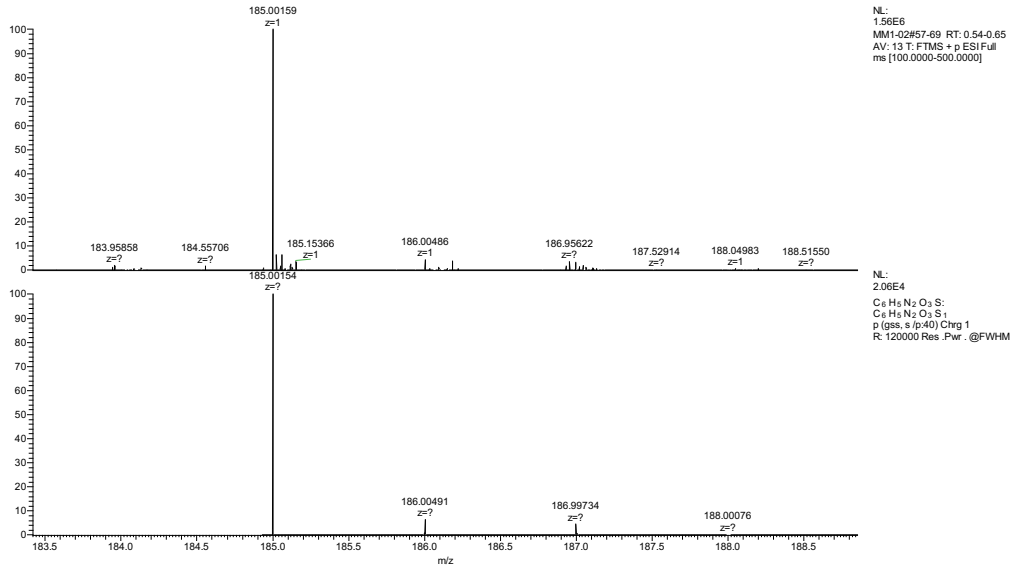

Fig. S10 HRMS spectrum of 4-SBD.

Colorimetric assay of 4-SBD reactivity. To confirm the reactivity of 4-SBD at any time, a solution of 4-SBD (1 $mg \cdot ml^{-1}$) in 0.1 M aqueous HCl was mixed with dimethylaniline to obtain methyl orange, a common pH indicator. After mixing, the colorless mixture rapidly turned red or yellow depending on the pH, which is indicative of methyl orange. Mixing a solution of 4-sulfophenolic acid, the major degradation product of 4-SBD, with dimethylaniline did not result in any color change.

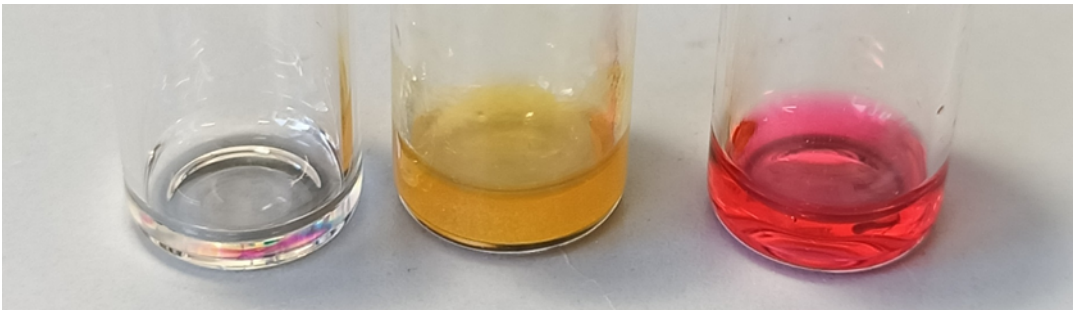

Fig. S11 Optical images of SBD-dimethylaniline solutions. From left to right: aqueous mixtures of dimethylaniline with 4-sulfophenolic acid, dimethylaniline with 4-SBD at pH > 4.4, and dimethylaniline with 4-SBD at pH < 3.1. pH-dependent colorization after mixing dimethylaniline and 4-SBD indicate that methyl orange has been successfully formed.

2.2 Single-crystalline graphene growth and characterization.

Large-area high-quality single-crystalline graphene samples were epitaxially grown on Cu(111) foils via the chemical vapor deposition (CVD) method[18]. Decimeter scale commercially available polycrystalline Cu foils were placed in a homemade low-pressure CVD system, which is equipped with a 6-inch quartz tube. An asynchronous

heating process was conducted and therefore a temperature gradient was then applied to the Cu foils, which promotes the Cu grain growth and leads to the formation of large-area Cu(111) single crystal[19]. The heating and annealing process was carried out under Ar gas (1000 sccm, 500 Pa), in which trace amounts of oxygen could clean the surface of Cu foils and passivate the active sites of Cu to suppress the adlayer formation and nucleation density. Subsequently, keeping the temperature at 1020 °C, graphene growth proceeded under a gas mixture of H_2 (500 sccm) and CH_4 (0.8 sccm). Typical SEM images of as-grown graphene on Cu(111) with 30 and 60 mins are shown in Fig. 2B. The well-aligned hexagonal graphene domains indicate the unidirectional orientation of graphene lattice and free of grain boundaries in the seamlessly stitched graphene film. Transmission electron microscopy (TEM) and selected area electron diffraction (SAED) measurement (JEM-2100, at 200 keV electron energy) were also conducted on the as-obtained graphene samples, which were transferred onto TEM grids (3 mm in diameter) without polymer transfer medium. As shown in Fig. S12, a series of SAED patterns collected on different positions across the graphene sample are with the same orientation, which implies the single-crystal nature of as-grown graphene. Furthermore, the intensity profile of the diffraction pattern along the red dashed line in Fig. S12f indicates that it is monolayer graphene.

We also characterized the transferred graphene on SiO_2/Si substrate by using optical microscopy (OM) and Raman spectroscopy (Fig. S13). The high uniformity of optical contrast in OM image (Fig. S13a) and noise-level D-band intensity in Raman spectra (Fig. S13b) confirm the high quality and uniformity of as-grown monolayer graphene

[20,21].

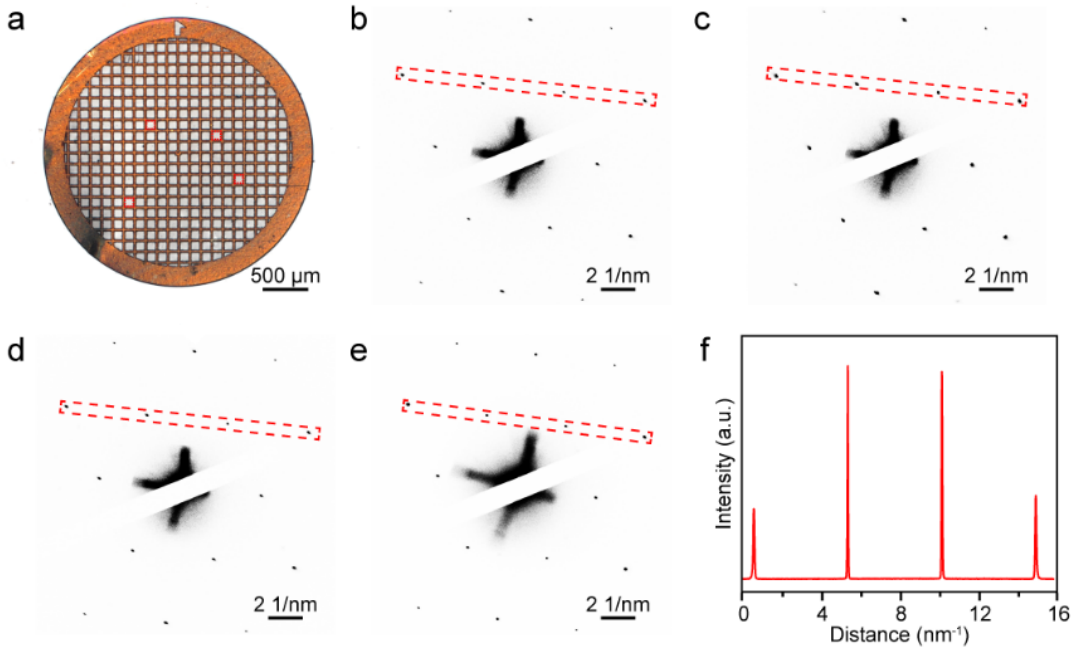

Fig. S12 Characterization of graphene lattice orientation. (a) Optical microscope image of the suspended graphene transferred onto a TEM grid. **(b-e)** Typical SAED patterns of the suspended single-crystal graphene measured at the marked red quadrans position in (a). **(f)** The intensity profile of the diffraction pattern along the red dashed line in (e), indicates a typical graphene lattice size.

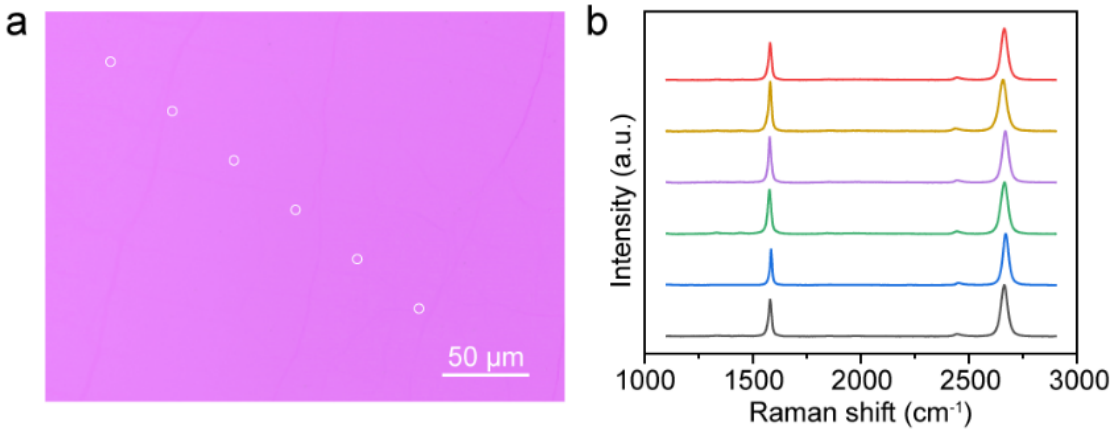

Fig. S13 Characterization of the single-crystalline graphene film. (a) Optical microscopy image of monolayer graphene transferred onto a SiO_2/Si substrate. **(b)** Representative Raman spectra of the as-transferred graphene measured at the marked position in (a).

2.3 Characterizations of single-crystalline CVD graphene after 4-SBD treatment (Raman spectroscopy, XPS, AFM, and HRTEM).

Raman spectroscopy

Raman spectra were recorded on a WITec confocal Raman spectrometer with a 457 nm laser and a 100× objective under 1.5 mW laser power.

For Nafion/graphene samples, we spin-coated a Nafion solution (~5% D521 from Fuelcellstore) on single-crystalline graphene on a copper foil at 2000 rpm for 1 min followed by baking on a hotplate at 60 °C for 30 mins to fully remove the solvent. Then, the Cu film was etched away by floating the copper/graphene/Nafion stack on an 0.5M aqueous solution of ammonium persulfate (APS, from Sigma-Aldrich) in a glass petri dish. Nafion/graphene was then rinsed by transferring the film onto the water-air meniscus (again floating) in a fresh ultrapure water bath for 20 mins. This procedure was repeated 3 times. For the 4-SBD treatment, Nafion/graphene was floated on the 4-SBD solution (0.1 $mg \cdot ml^{-1}$) in a Petri dish for the time indicated. Then, the samples were floated on 0.1 M HCl for 40 mins and rinsed 3 times for 20 mins each time in ultrapure water. Finally, the Nafion/graphene stack was transferred to a SiO_2/Si wafer (with 285 nm thermal oxide layer, purchased from Siegert Wafer) before Raman

characterization. Fig. S14 shows the mapping of the intensity ratio of the D peak and 2D peak over the G peak from the Raman spectrum indicating the homogeneity of 4-SBD grafting.

For graphene/SiO_2 samples without a Nafion layer, CVD graphene was transferred onto a silicon wafer with 285 nm SiO_2, using spin-coated poly(methyl methacrylate) (PMMA) as a carrier[22]. In this process, ~50 µl PMMA solution (6% in anisole, AR-P 662.06, purchased from All resist GmbH), was drop-casted on ~1.5 cm^{-2} graphene on Cu foil. The PMMA was then dried by spin-coating at 4000 rpm for 1 min. The resulting PMMA/graphene/Cu was baked at 80 °C for 30 mins to remove the solvent. Afterward, PMMA/graphene was obtained by etching the Cu in 0.5M APS and rinsing in ultrapure water as mentioned previously. PMMA/graphene was then transferred to a SiO_2/Si wafer (~4 cm^{-2}). PMMA/graphene on the wafer was baked at 120 °C for 30 minutes to ensure a good adhesion between the graphene and the SiO_2 layer[23] followed by 15 minutes of immersion in acetone to remove PMMA (acetone rinsing was carried after the wafer cooled down to room temperature). To further clean the PMMA residue on the graphene surface, fresh acetone, isopropanol, and ethanol were stepwise flushed using a squeezing bottle through the top surface of the graphene. Then the graphene/wafer was baked at 120 °C for half an hour to further improve the adhesion between the graphene and SiO_2 surface. Next, a drop of isopropanol (~5 µl for 1 cm^{-2} of graphene) was added on top of the sample to avoid the direct surface tension force when dipping the sample into a 4-SBD solution. Then the samples were immersed in the 4-SBD solution. Before the Raman characterization, samples were rinsed in

ultrapure water several times and dried in air.

Mapping of the intensity ratio (2D peak and G peak, I_{2D}/I_G) confirmed that the functionalization is uniform over the single-layer area. While the reactivity of the multi-layer is suppressed, indicated by a very low D peak intensity (Fig. S15). Previously, the hindering of diazonium reactivity by the multilayer was discussed as an effect of the substrate[24,25]. Therefore, we assumed that the 4-SBD treatment for the preparation of SO_3^--graphene only works for the monolayer graphene. Fig. S16 shows the relationship between 4-SBD treatment time and Raman spectra for graphene on SiO_2/Si.

For the defect density, though there were reports to conduct quantitative estimation via I_D/I_G and the size of vacancy, the estimation is based on the vacancy-like defects[26]. In our samples, no D' peak was not found and this further proved that the sulfophenyl groups were covalently grafted to graphene via sp^3 distortion.

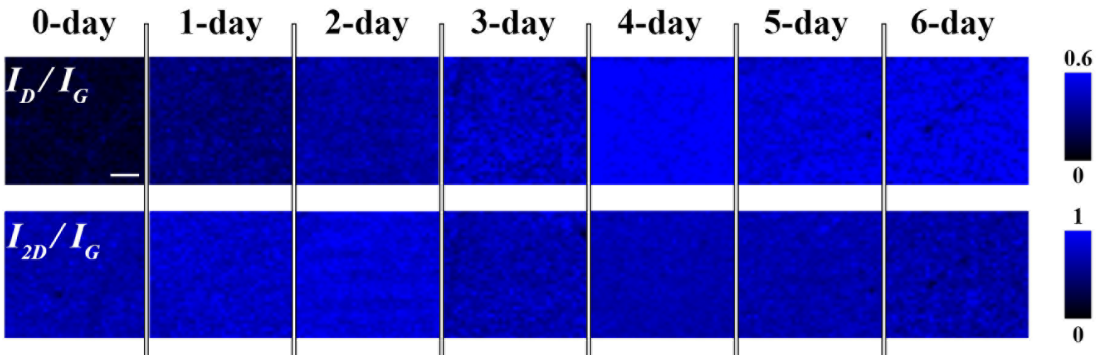

Fig. S14 Raman mapping of peak intensity ratios, I_D/I_G and I_{2D}/I_G, images of Nafion/graphene after floating on SBD solution for 0 to 6 days. The scale bar is 2 μm.

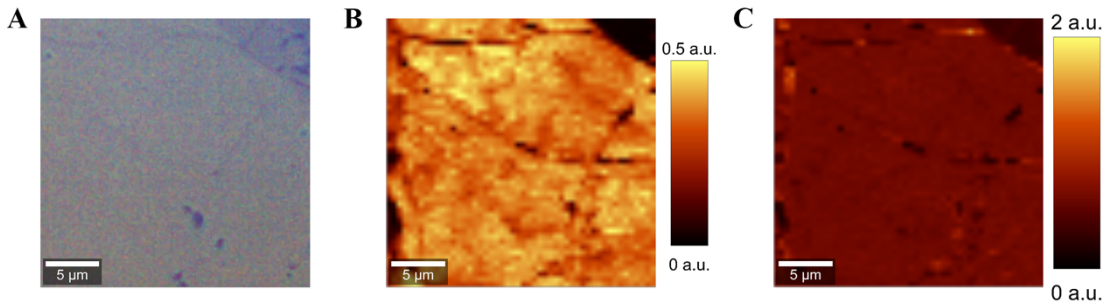

Fig. S15 Graphene on a SiO_2/Si wafer after 4 days of 4-SBD treatment. **(A)** Optical microscopy image. **(B)** Raman mapping of the intensity ratio of D peak over G peak. **(C)** The intensity ratio of 2D peak over G peak.

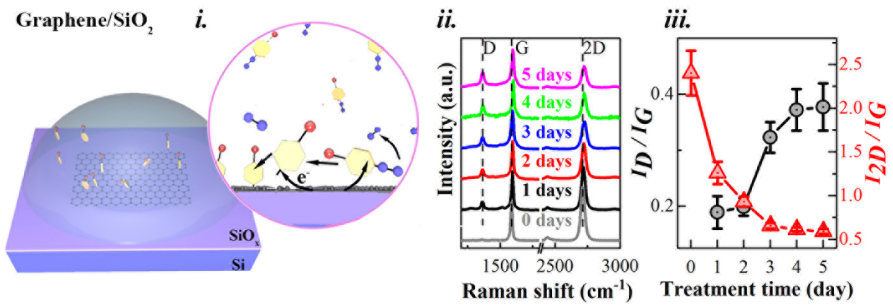

Fig. S16 Raman analysis of graphene on SiO_2/Si. Sii) Illustration of graphene on SiO_2/Si reacting with a solution of 4-SBD (1 mg·ml^{-1} SBD in aqueous 0.1 M HCl). ii) Raw Raman spectra for graphene on a SiO_2/Si substrate after 0-6 days of floating incubation with 4-SBD. Raman spectra were recorded over a 10×10 μm area using a 457 nm laser set to 1.5 mW power to avoid any laser-induced damage to the SO_3^--graphene. We normalized the spectra by the intensity of the G peak to facilitate a comparison of the D and 2D peaks. iii) Plot of I_D/I_G and I_{2D}/I_G versus 4-SBD treatment time derived from panel Aii).

X-ray photoelectron spectroscopy (XPS)

Measurements were performed with a Thermo Fisher VG Escalab 250 spectrometer as part of the cluster tool DAISY-SOL. It was equipped with a monochromatic X-ray source (Al Kα= 1486.6 eV) set at 15 mA and 15 kV with a spot size of 650 µm in diameter. The pressure inside the analytical chamber was monitored below 2×10^{-9} mbar. Except where otherwise stated, survey spectra were acquired with a pass energy of 50 eV, a step size of 0.1 eV, and a dwell time of 50 ms per measurement point. The detailed scans were acquired with lower pass energy (10 eV) and lower step size (0.05 eV); up to 50 scans were made to increase the signal-to-noise ratio. Metallic foils (Ag, Au, Cu) were cleaned by Ar sputtering (3 kV for 180 s) and used for the spectrometer calibration (Fermi edge of Ag at 0.0 eV, Au $4f_{7/2}$ = 84.0 eV, Ag $3d_{5/2}$ = 368.3 eV, Cu $2p_{3/2}$ = 932.7 eV). The Fermi level of the cleaned silver was also used to determine an instrumental resolution of 0.35 eV for XPS (pass energy of 10 eV). After XPS spectra acquisition, they were slightly adjusted (one sample with a shift of 0.4 and the other +/- 0.1 eV) using the C1s sp^2 peak at binding energy (BE) of 284.5 eV. For measuring the 4-sulfonatebenzendiazonium (4-SBD) powder on foil, a flood gun was required to bring the adventitious carbon state as close as possible to 284.8 eV; despite that, charge the correction of the spectra to lower BE (≈1.8 eV) were made afterward (Fig. S17).

Interestingly, for the graphene samples immersed in solutions containing 1 and 0.1 $mg \cdot ml^{-1}$ of SBD, the sp^3C/sp^2C ratios increase with the concentration of the solution and with the content of SO_3^- detected at the near surface of the graphene samples. A 4-SBD treatment with 10 times less concentrated solution (0.1 $mg \cdot ml^{-1}$) leads to a reduction of the XPS peak intensities demonstrating that there are 1.5-3.7 times fewer

SO_3^- groups grafted to the graphene basal plane (Table S2). Besides, the two additional C states are assigned to C-N (BE≈ 286.7 eV) and O-C-O (BE≈289.1 eV)[27]. The small amount of sp^3 content inside the pristine sample is assigned to unavoidable C-C contamination of the samples during the polymer-assisted transfer procedure.

For the quantitative chemical analysis and the binding energy (BE) shifts, spectra were analyzed with CasaXPS (version 2.3.19PR1.0) and the Scofield relative sensitivity factor (R.S.F)[28]. Spectra were fitted by first, subtracting spectral background using a Shirley-type function using weighted least-squares method and model curves (Voigt functions of 70% Gaussian and 30% Lorentzian for all the peaks and an asymmetric Lorentzian "LA(1.2,2.5,5)" for the sp^2 carbon. The fitting methodology has been inspired by the work of Biesinger[29]. Full half-width maxima (fwhm) of the sp^2 C and sp^3 C were constrained between 0.4-0.8 eV and 0.9-1.3 eV, respectively. The fwhm of the C-N and O-C-O peaks were constrained to be equal to the one of the sp^3 C +/- 0.05 eV. The N=N, NH_2, and NO_x peaks were also constrained to have the same fwhm +/- 0.05 eV. The position of the C-N and the O-C-O peaks were, respectively, constrained to be at 1.3-1.7 eV and 3.8-4.3 eV higher energy than the sp^3 C peak.

In the N1s core level spectra, three states were identified at roughly 400.3 eV which is assigned to the azo-N=N- of the SBD molecule, or to adsorbed N_2 as it is the case for the pristine sample, 402 eV which refers to -NH_2 or -NH_3^+ probably formed after oligomerization, and 406.1 eV indicates oxidized nitrogen[30]. -NH_2 and oxidized nitrogen are unexpected indicating unknown side reactions besides radical coupling and

azo coupling. The peak in the S2p spectrum centered at 168 eV corresponds to $-SO_3^-$ [31], which was also observed for the powder SBD precursor (Fig. S17C).

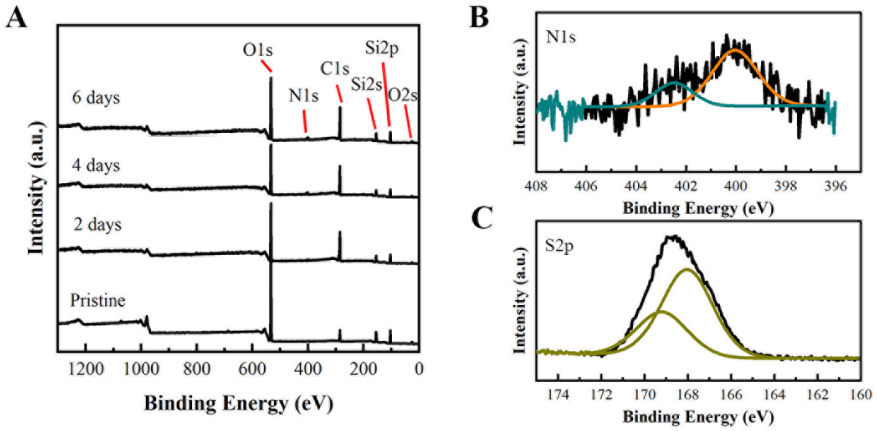

Fig. S17 XPS survey spectra and N1s/S2p spectra of 4-SBD powder. (A) Survey spectra of pristine graphene and graphene after 2 days, 4 days, and 6 days 4-SBD treatment. **(B)** N1s spectrum and **(C)** S2p spectrum of 4-SBD powder.

Table S2: Datasheet of XPS analysis.

Duration of treatment	4-SBD concentration ($mg \cdot ml^{-1}$)	Peaks relative concentration (%)								sp^3C/sp^2C ratio
		S2p	C1s				N1s			
		SO_3^-	sp^2	sp^3	C-N	O-C-O	N=N	NH_2	NO_x	
pristine		0	69.9	13.0	9.2	3.3	3.9[a]	0.7[a]	0	0.19
2 days	1	2.6	36.7	36.3	13.1	9.2	1.2	0.6	0.4	1.00
4 days		5.2	55.8	19.7	10.6	3.2	3.1	0.6	1.9	0.35
6 days		6.3	58.9	17.7	7.6	2.9	3.3	2.0	1.5	0.30
2 days	0.1	1.7	39.4	34.0	13.9	7.5	2.4	0.7	0.5	0.86
6 days		1.7	39.5	33.3	13.8	10.2	0.9	0.4	0.3	0.84

[a] Nitrogen content in the pristine sample is assigned to adsorbed N_2.

Atomic force microscopy (AFM)

AFM images were recorded using a JPK NanoWizard Ultra Speed microscope and the obtained data was processed using the JPK SPM Data Processing software. All experiments were performed using a silicon probe (Olympus, OMCL-AC240R3) with a nominal resonance frequency of 70 kHz. The images were all scanned and recorded (with a resolution of 1024x1024 pixels) in intermittent contact mode in the air at room temperature. For each incubation time, three individual regions were recorded and the surface roughness was calculated from the combined three regions. The AFM characterization was conducted with graphene on the TEM grid to allow the characterization over free-standing graphene, which is prepared by the following steps. A droplet of isopropanol was added to the TEM grid (carbon film on top), and a piece of flat graphene/Cu film was gently put on the droplet (graphene side on bottom). Then, the sample was dried at room temperature. After the drying out of isopropanol, the sample was flipped over and floated on 0.5 M APS solution to fully etch away Cu film. Then the sample was floated on ultrapure water for 20 mins and this procedure was repeated for 3 times. The as-prepared sample was floated on 0.1 M HCl to preclude the influence of water and HCl on the graphene morphology (shown in Fig. S18 & 19). Then the samples were treated with 4-SBD (1 $mg \cdot ml^{-1}$ in 0.1 M HCl solution) in the same manner mentioned above for a specific time, followed by the rinse of 0.1 M HCl after treatment.

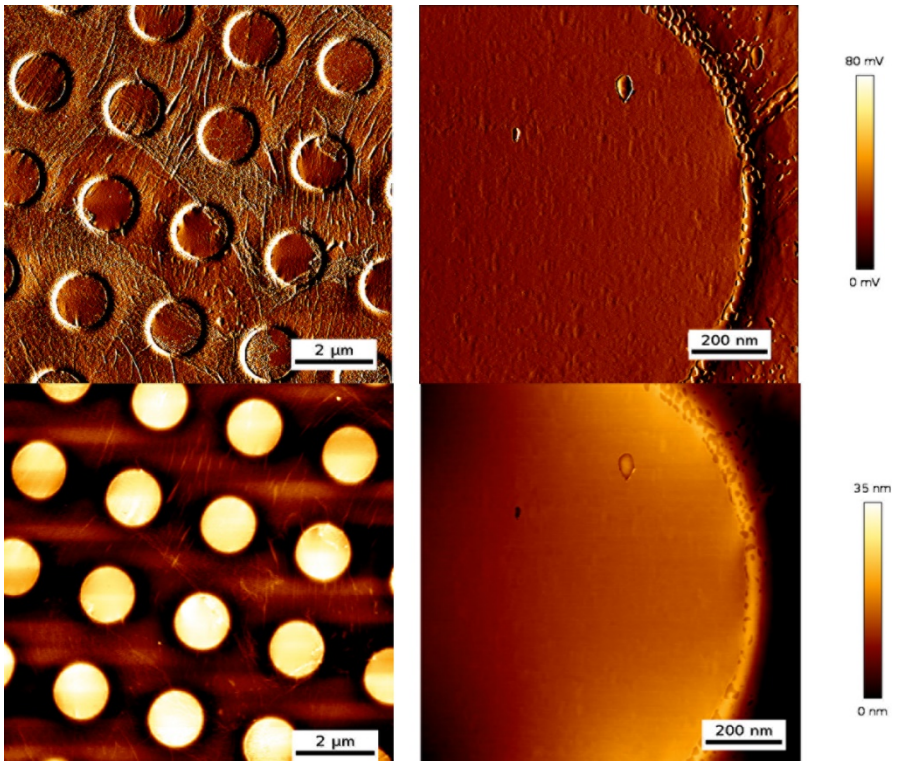

Fig. S18 AFM images of CVD graphene after floating on 0.1 M HCl solution for 6 days.

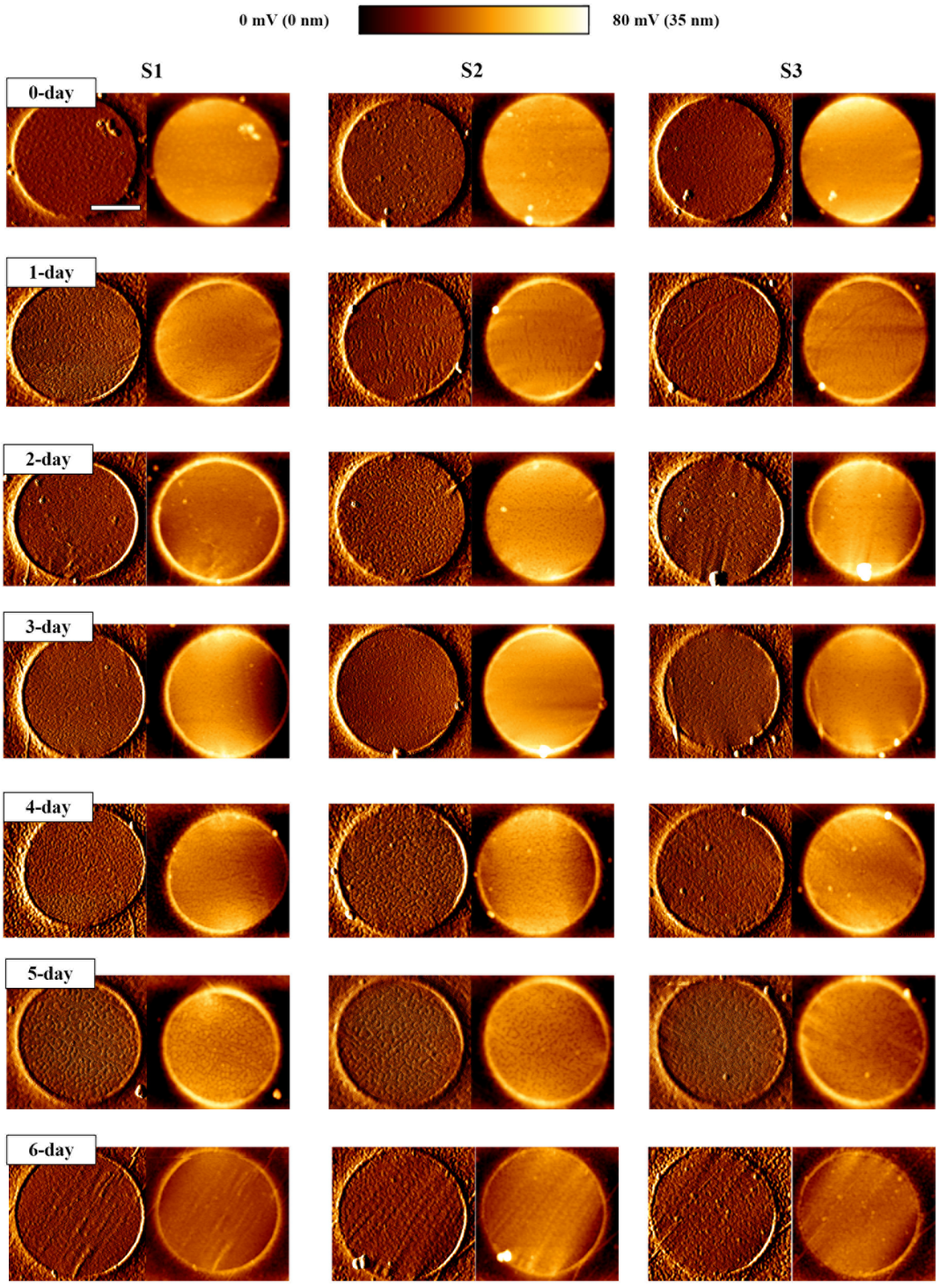

Fig. S19 AFM images of graphene samples free-standing on TEM grids. For each of treatment time, three random positions were selected for the AFM mapping. The left image of each set is the error image and the right image is the height image. Scale bar: 500 nm.

High-resolution transmission electron microscopy (HRTEM) characterization.

For the consistency of samples, the samples for HRTEM characterization are prepared in the same manner as samples for AFM characterization. HRTEM images were acquired with the image-side CC/CS-corrected SALVE microscope operated at 80 kV with a resolution of 76 pm (SALVE: Sub-Angstrom Low-Voltage Electron Microscopy). Data acquisition was conducted on a Ceta CMOS camera. We conducted HRTEM characterization of SO_3^--graphene with all three batches of 4-SBD used in this work (Fig. S20 for batch 1, Fig. S21 for batch 2, and Fig. S22 for batch 3). From all these observations, we did not find any vacancy-like defects generated after 4-SBD treatment.

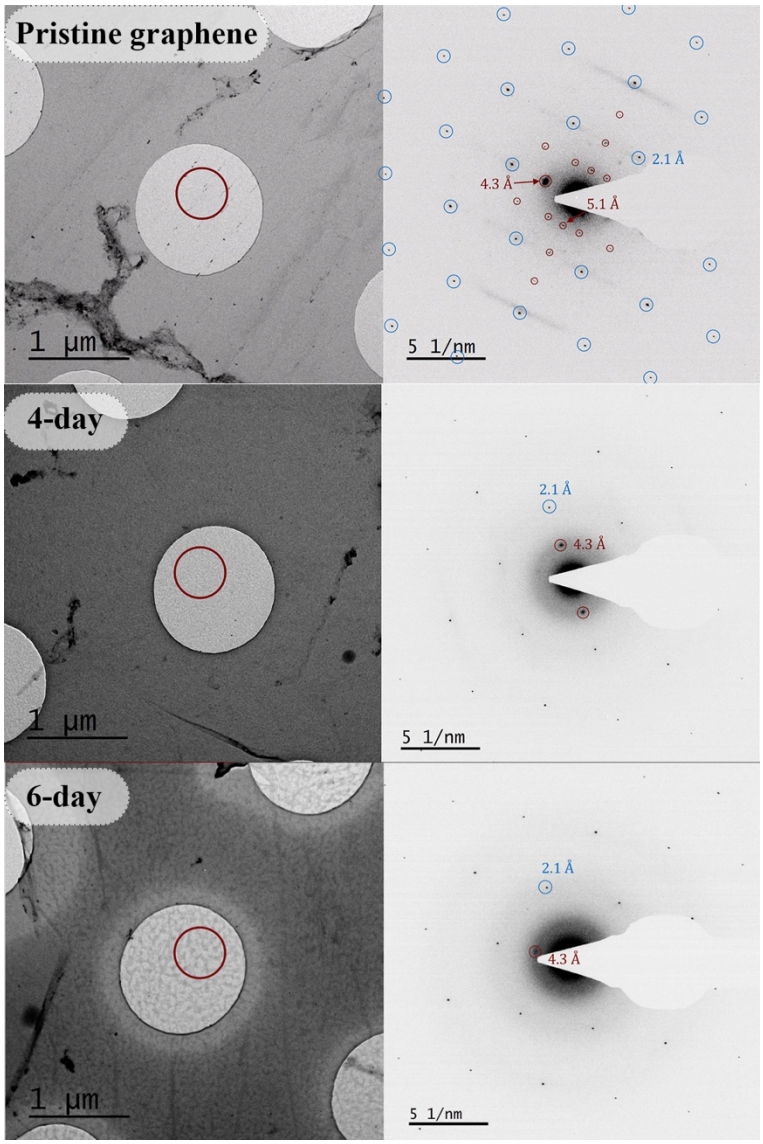

Fig. S20 TEM images of graphene treated with 4-SBD batch 1. TEM image were recorded with diffraction pattern of pristine CVD graphene and SO_3^--graphene after 4 days and 6 days 4-SBD (1 mg·ml^{-1} in 0.1 M HCl) treatment.

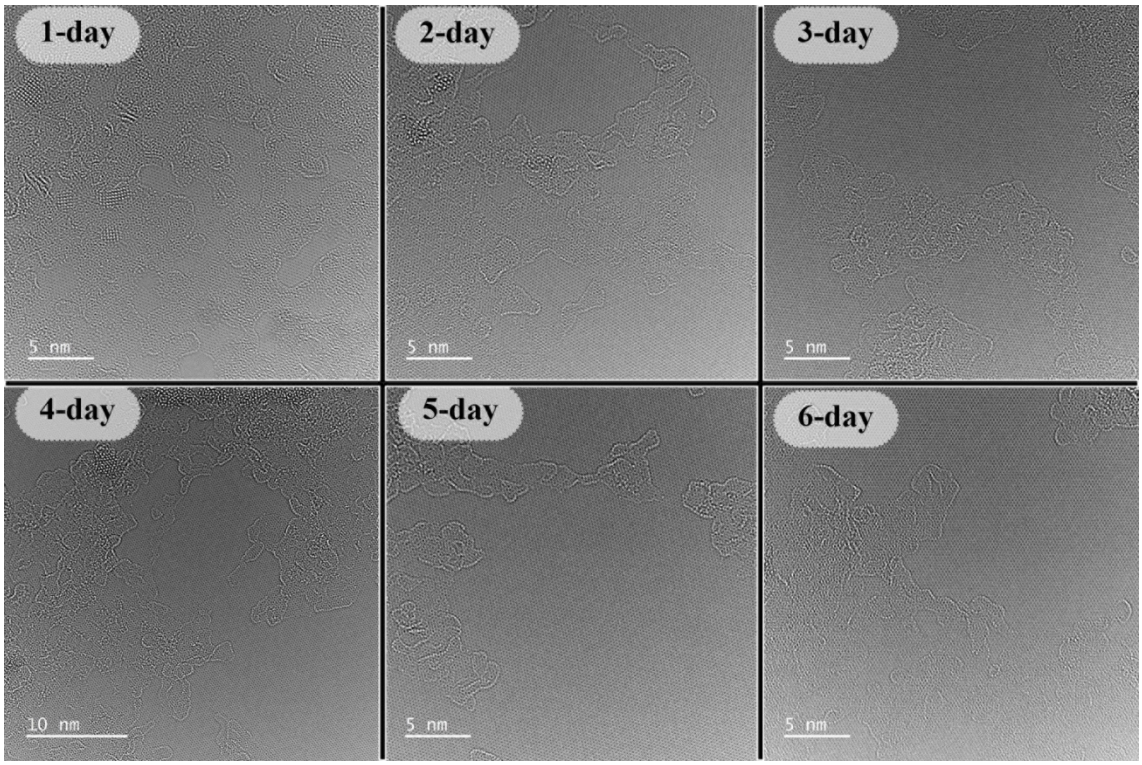

Fig. S21 TEM images of graphene treated with 4-SBD batch 2. HRTEM images were recorded of CVD graphene after 1 to 6 days of 4-SBD (1 mg·ml^{-1} in 0.1 M HCl) treatment.

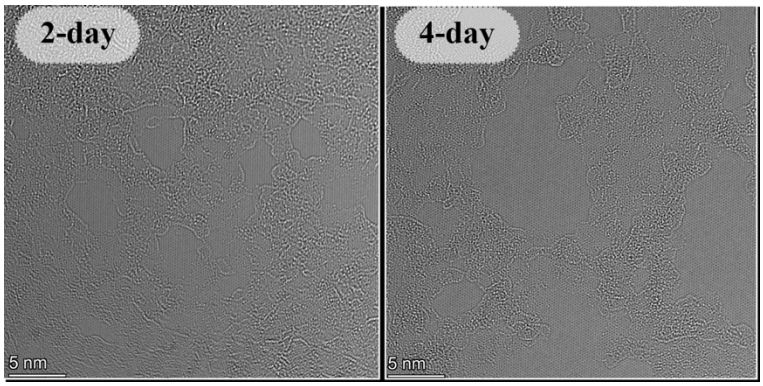

Fig. S22 TEM images of graphene treated with 4-SBD batch 3. HRTEM images were recorded of CVD graphene after 2 and 4 days of 4-SBD (1 mg·ml^{-1} in 0.1 M HCl) treatment.

3. Direct methanol fuel cell measurements.

3.1 Membrane-electrode assembly fabrication.

A single-crystalline CVD graphene membrane was used in a DMFC application, where cracks or defects were minimized during the chemical vapor deposition process. Graphene-based membranes were prepared with a porous polycarbonate (PC) membrane as a support (Nuclepore track-etch membrane with a pore diameter of 3 μm, Whatman), and a proton-conducting ionomer (Nafion dispersion D521, Fuelcellstore) was used as a stabilizer to prevent direct contact between the graphene lattice and electrodes.

To prepare the membrane, CVD graphene on Cu (1.2 by 1.2 cm^2) was first spin-coated with the Nafion solution (D521) at 2000 rpm for 1 minute and then baked at 80 °C for 30 minutes on a hot plate. The Nafion/graphene/Cu was then placed on a piece of PC membrane, and the Cu was etched by floating the Nafion/graphene/Cu/PC sample on a 0.5 M APS solution in a petri dish. The sulfophenylation with SBD was conducted by floating Nafion/Graphene/PC on the SBD solution (1mg/ml, 0.1 M HCl). The resulting Nafion/graphene/PC composite membrane was rinsed and stored in 0.1 M HCl before being fixed between two PTFE gasket sheets using soft replica rubber (Reprorubber Thin Pour, Flexbar Machine Corp.). A Nafion solution was drop-casted twice onto the backside of the PC support, followed by baking at 80°C for 30 minutes each time (to act as a mechanical contact buffer during assembly of the fuel cell and following the

compression from the electrodes). The anode, with a Pt/Ru loading rate of 4 mg cm^{-2}, and the cathode, with a Pt loading rate of 4 mg cm^{-2} (Fuelcellstore), were then put on the sides of the MEA before the measurements. Fig. S23 depicts the assembly steps.

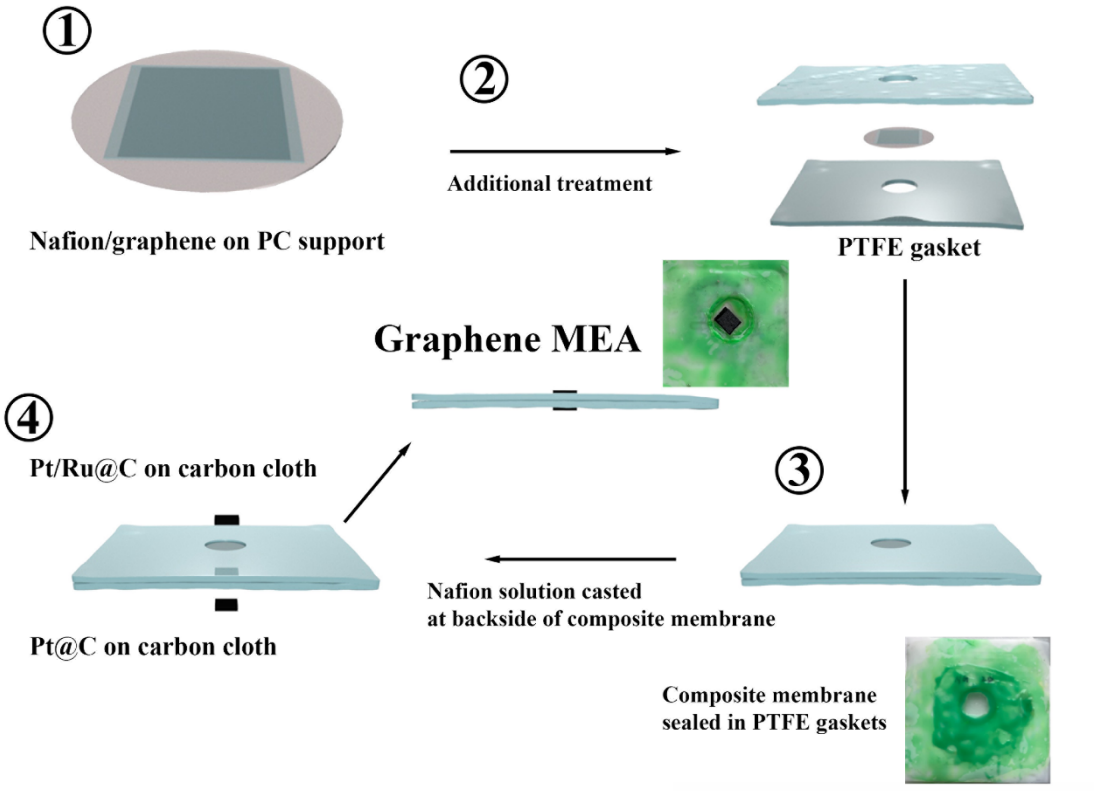

Fig. S23 Graphene MEA preparation. The samples were floated directly on the 4-SBD solution and subsequently transferred to a 0.1 M HCl solution before use. Next, the sample was fixed between two PTFE gaskets with a circular window of 1 cm using soft replica rubber, ensuring that only the area covered by the graphene sample was exposed. Finally, the electrodes were placed directly on both sides of the assembly before the measurements were taken in the DMFCs.

3.2 DMFC operation.

All electrochemistry measurements were conducted using a potentiostat (PGSTAT204) equipped with an electrochemical impedance spectroscopy model (FRA32M) and operated using the Nova software.

DMFC measurements were carried out using an electrolyzer from Dioxide Materials, with a titanium anode plate and a cathode made from 904 L stainless steel. The cells were operated using a methanol/water mixture at a flow rate of 30 ml min^{-1} passing through the anode. To ensure the reliability of all measurements, all cells were started with 5 rounds of CV scanning from 0 to 1.5 V at a speed of 10 mV s^{-1}, and cathode starvation was performed by floating N_2 gas instead of O_2, followed by 20 minutes of running the cell at 200 mV. The open circuit voltage was determined by fixing the cell current to 0 and recording it after 5 minutes with no voltage variation. After the cell was fully stabilized and the current variation (under 200 mV) was less than 10 μA min^{-1}, the polarization curves were obtained by linear sweep from open circuit voltage to short circuit voltage at a 10 mV s^{-1} scan rate. The resistance was determined by reading the intercept from the Nyquist plot of the electrochemical impedance spectrum, which was measured with frequencies from 1 KHz to 0.1 Hz and 10 mV amplitude under an open circuit. Data were acquired using three independent samples for reproducibility check, and the error bars indicate the maximum and minimum derivation instead of standard derivations for directly showing the experimental results.

In addition to using 1 M and 5 M methanol, we attempted to increase the fuel concentration to 10 M methanol. However, this resulted in significant dehydration of

the Nafion layer, causing a substantial leakage of methanol and ultimately leading to the destruction of the MEA.

We spin-coated a Nafion ionomer layer onto a flat Cu foil without graphene and then transferred it onto a porous PC membrane by etching away the Cu, floating the Nafion/Cu/PC stack on a Cu etchant. The Nafion/PC membrane was subsequently rinsed in ultrapure water and 0.1 M HCl, following the same procedure used for fabricating the Nafion/graphene/PC membranes in our study. Our results showed that the Nafion ionomer alone was highly permeable to the methanol/water mixture. In DMFC tests, this led to significant methanol crossover, causing near-zero cell current and complete activation failure (see Fig. S24).

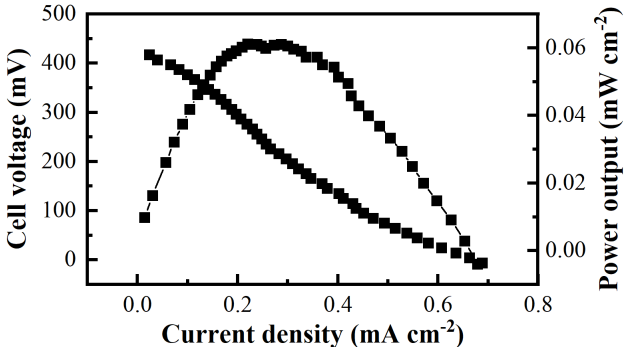

Fig. S24. DMFC performance of a Nafion spin-coated PC membrane.

The graphene membrane samples underwent a thorough rinsing process in ultrapure water (Fig. S25) and 0.1 M HCl (Fig. S26). For that, graphene samples were floated on ultrapure water and 0.1 M HCl for 2 to 12 days and tested in a DMFC at 60 °C. We did not measure a significant change in power output at a temperature of 60 °C. This observation suggests that water and 0.1 M HCl only (*i.e.,* without SBD), result in no

significant influence on the performance of pristine graphene membranes in terms of their maximum power output within DMFCs, suggesting the effect to be attributed to the functionalization of graphene with SBD.

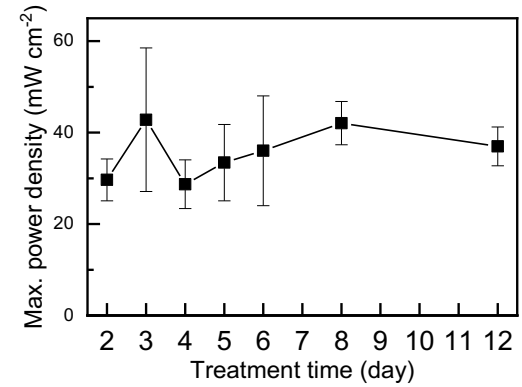

Fig. S25 Maximum power output of Direct Methanol Fuel Cells (DMFCs) with graphene membranes floated on pure water. Graphene membranes were floated on ultrapure water using the same conditions applied for the SBD treatment. The fuel cell tests were operated at 60 °C, with same flow rate of 1 M methanol solution and oxygen as tests conducted with SO_3^--graphene membranes.

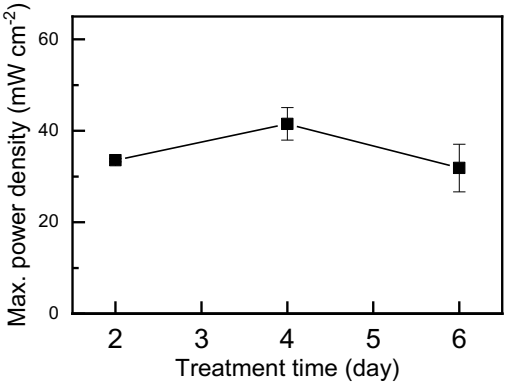

Fig. S26 Maximum power output of Direct Methanol Fuel Cells (DMFCs) with graphene membranes floated on 0.1 M HCl solution. Graphene membranes were floated on 0.1 M HCl using the same conditions applied for the SBD treatment. The fuel cell experiments were performed at 60 °C, with same flow rate of the 1 M methanol solution and oxygen as experiments conducted with SO_3^--graphene membranes.

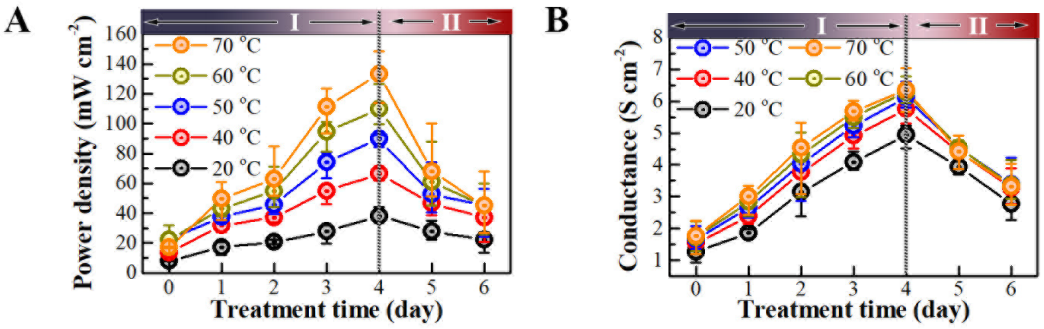

Fig. S27 Power output and membrane conductance of DMFCs measured with graphene membranes. (A) Maximum power density of DMFCs as a function of SBD treatment time for SO_3^--graphene membrane under operating temperature from 20 °C to 70 °C with 1 M methanol/water as fuel. **(B)** Membrane conductance of DMFCs with 1 M methanol and SO_3^--graphene membranes after treatment time from 0 to 6 days under operation temperatures from 20-70 °C.

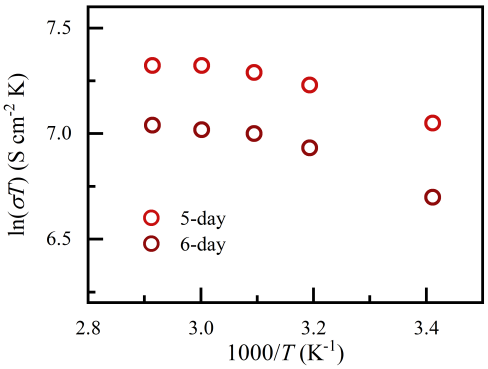

Fig. S28 Supplementary Arrhenius analysis of conductance. ln(σ*T*) as a function of the inverse of temperature for graphene membranes after 5 days and 6 days 4-SBD treatment.

Table S3: Datasheet of Arrhenius behavior analysis

T (K)	1000/T (K^{-1})	0-day		1-day		2-day		3-day		4-day		5-day	
		σ (S cm^{-2})	ln(σT)	σ (S cm^{-2})	ln(σT)	σ (S cm^{-2})	ln(σT)	σ (S cm^{-2})	ln(σT)	σ (S cm^{-2})	ln(σT)	σ (S cm^{-2})	ln(σT)
293.15	3.41	1.13	5.81	1.86	6.30	3.15	6.83	4.08	7.09	4.94	7.28	3.93	6.70
313.15	3.19	1.39	6.08	2.39	6.62	3.77	7.08	4.91	7.34	5.75	7.50	4.41	6.93
323.15	3.09	2.30	6.61	2.65	6.75	4.04	7.17	5.22	7.43	6.12	7.59	4.53	7.00
333.15	3.00	2.19	6.59	2.83	6.85	4.32	7.27	5.50	7.51	6.29	7.65	4.54	7.02
343.15	2.91	1.81	6.43	3.01	6.94	4.55	7.35	5.68	7.58	6.35	7.69	4.41	7.04

Next, we analyzed short circuit currents as a function of temperature. We plotted ln($I \times T$) vs T^{-1} for pristine and after 1, 2, 3 and 4 day (Fig. S29A) and 5-6 days (Fig. S29B) of SBD treatment. For all samples, ln($I \times T$) follows a linear trend with T^{-1}.

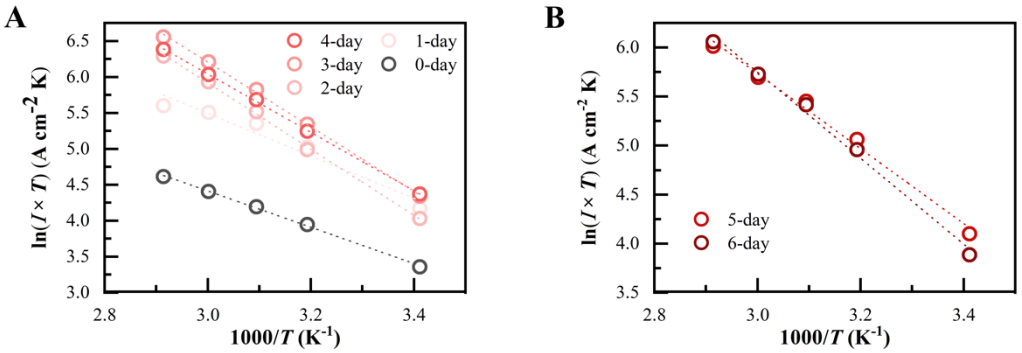

Fig. S29 Supplementary Arrhenius analysis of current. ln($I \times T$) as a function of the inverse of temperature for graphene membranes with 4-SBD treatments from 0 to 6 days.

To explore potential differences in DMFC performances between the standard (*i.e.,* forward) membrane assembly, we tested devices with the sulfophenylated membrane side facing the anode at 60 °C (Fig. S30). Such device showed a slight difference in conductance, compared to the forward membrane assembly (*i.e.,* 5.4 S·cm^{-2} *vs.* 5.6 S·cm^{-2}, normalized to the electrode area). However, we observed a small decrease in the open circuit voltage (580 mV *vs.* 630 mW) and the maximum power output (70

mW·cm^{-2} *vs.* 109 mW·cm^{-2}), compared to the forward membrane assembly. Since the conductance values are similar in both assemblies, we speculated the differences to be caused by the hydrostatic pressure induced delamination and methanol solution leakage.

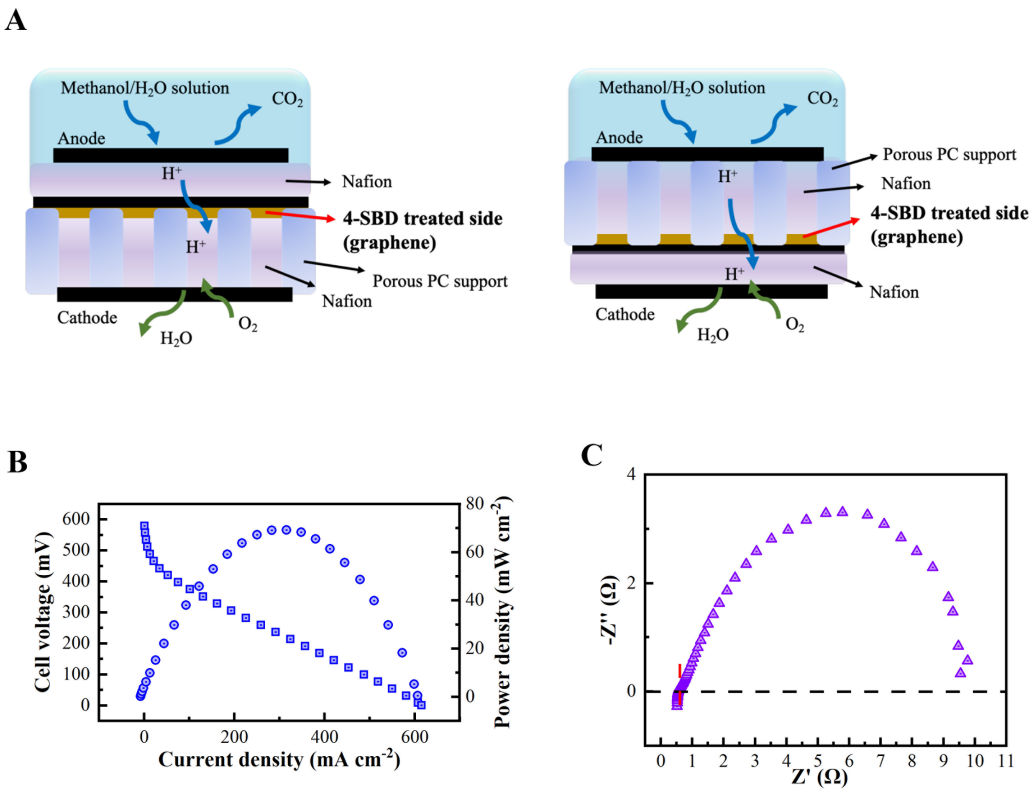

Fig. S30 Comparison of DMFC performances for SO_3^--graphene facing the anode (reverse assembly) *vs.* SO_3^--graphene facing the cathode (forward assembly). (A) For the forward assembly (**left**), which has been applied in DMFC measurements in the main text, the 4-SBD treated side of graphene was facing the cathode via the channels of porous PC support. In this comparison, (the reverse assembly, **right**), the 4-SBD treated side of graphene was facing the anode via the channels of porous PC support. Power-current density (*P-I)* and voltage-current density (*V-I)* curves **(B)** and the Nyquist plot of EIS measured at 200 mV **(C)** of the DMFC with the ***reverse membrane assembly.*** In this measurement, the proton was transported from the sulfophenylated

side to the untreated side. The DMFC was operated with 1 M methanol under 60 °C.

3.3 Methanol crossover and fuel efficiency estimation.

The performance of a DMFC is influenced by methanol crossover in three major ways: it can poison cathode catalysts, reduce methanol efficiency, and decrease cell voltage due to a mixed potential at the cathode. To assess the membrane's properties, we investigated the methanol crossover behavior of an SO_3^--graphene membrane. Methanol crossover rate (J_m) is caused by three major effects: gradient diffusion resulting from concentration differences, electro-osmotic drag, and hydraulic pressure based on liquid pressure, which can be expressed as follows:

$$J_m = D\frac{\Delta C}{\delta_m} + n\frac{I}{F} + \frac{K_m \rho \Delta P}{\mu M_{H_2O}\delta_m} = \alpha\frac{I}{F} \qquad (2)$$

Where D is the diffusivity of water in the membrane, δ_m is the membrane thickness, ΔC is the concentration difference, n is the electro-osmotic drag coefficient, I is the current density, F is Faraday's constant, K_m is the permeability through the membrane, ρ is the density of water, ΔP is the difference of liquid pressure, μ is the viscosity of the liquid, M_{H_2O} is the molecular weight of water, α is the overall coefficient[32]. With the correlation between the working current and methanol current, we could estimate the methanol crossover current under different working currents by:

$$I_{crossover} = I_{crossover,limit}\left(1 - \frac{I}{I_{shortcircuit}}\right) \qquad (3)$$

where $I_{crossover}$ is the methanol crossover current, $I_{crossover,limit}$ is the limit current obtained

from crossover current measurements, $I_{\text{shortcircuit}}$ is the short circuit current of DMFC and I is the working current[33,34]. The ratio of $I_{\text{crossover, limit,}}$ and $I_{\text{shortcircuit}}$ decides the slope of eq. 3 which is in positive correlation with the overall crossover coefficient, α. To further compare the fuel efficiency among samples, we also converted the methanol crossover current information by[35]:

$$\eta_{fuel} = \frac{I}{I+I_{crossover}} \quad (6)$$

and calculated the fuel efficiency with I of a DMFC measured under 200 mV and $I_{\text{crossover}}$ calculated from eq.3 under 200 mV. We observed that the fuel efficiency at 200 mV was due to the maximum power output being achieved around that voltage and the DMFC operating at an optimal state.

Therefore, we characterized the methanol crossover by oxidizing the methanol at the cathode. The methanol crossover current was measured by linear sweep voltammetry from 0 to 1.2 V against the cathode and anode at a scan rate of 5 mV s^{-1} with a methanol flow rate of 30 ml min^{-1} at the anode and nitrogen flow at the cathode. The limiting current is taken as an indicator of the methanol crossover rate.

Fig. S31A displays the I-V curves of a DMFC (red, cathode fed with oxygen) and oxidizing methanol crossover from the anode to the cathode (dark, cathode fed with nitrogen). The crossover current ($I_{crossover}$) represents the amount of methanol that has diffused from the anode to the cathode through the membrane. It is possible to estimate the diffusion efficiency by comparing $I_{crossover}$ with the short circuit current ($I_{shortcircuit}$)

using the expression $I_{crossover}$ / $I_{shortcircuit}$[32]. For the pristine graphene membrane, an increase in temperature from 20 to 70 °C results in a significant rise in methanol crossover, indicated by the ratio of $I_{crossover}$ / $I_{shortcircuit}$ increasing from 0.44 to 1.21. Remarkably, after functionalizing graphene with 4-SBD for 2-4 days, $I_{crossover}$ / $I_{shortcircuit}$ becomes constant over the entire range of operating temperatures (Fig. S31B), suggesting that the temperature has a more significant impact on activity than the methanol crossover rate. Additionally, the negligible variation in methanol crossover for samples treated with 2 to 4 days of 4-SBD at different temperatures indicates that the selective pathway dominates. For samples with 5 and 6 days of treatment, the variation with different temperatures is more significant since the selective pathway is partially blocked by the oligomerization of the diazonium compound. The different methanol crossover rates also explain the temperature dependence of the cell performance, as mentioned above. Fuel efficiency at 200mV (η_{200mV}), which is close to the potential at maximum power density, is a practical Parameter to evaluate the fuel cell performance[35]. This efficiency was obtained from the methanol crossover current and the working state cell current (Fig. S31C). For the 4-day SO_3^--graphene at 60 °C, η_{200mV} reaches ~79% at a current density of 457.5 mA cm^{-2}.

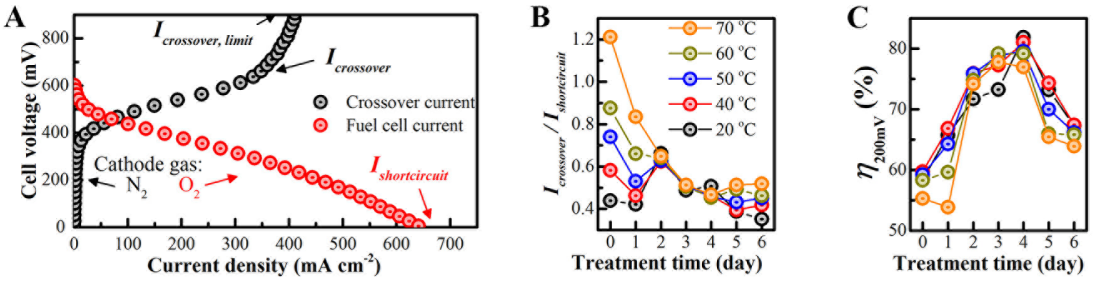

Fig. S31 Methanol crossover DMFCs with graphene and SO_3^--graphene at different temperatures. **(A)** Methanol crossover (black) vs. fuel cell current was measured on 4-day SO_3^--graphene (red) at 60 °C with 1M methanol as fuel. In the methanol crossover I-V curve, the diffusion-limited current *($I_{crossover,\ limit}$* plateau region intercepted with x-axis), and in the fuel cell I-V curve, the short-circuited (0 V output) is the maximum current of the DMFC ($I_{shortcircuit}$). **(B)** The ratio of limiting methanol crossover current over short-circuit cell current ($I_{crossover,\ limit}$ / $I_{shortcircuit}$) as a function of treatment time and under operating temperature from 20 to 70 °C. **(C)** Fuel efficiency at an output voltage of 200mV under operating temperature from 20 to 70 °C (the same color code as B).

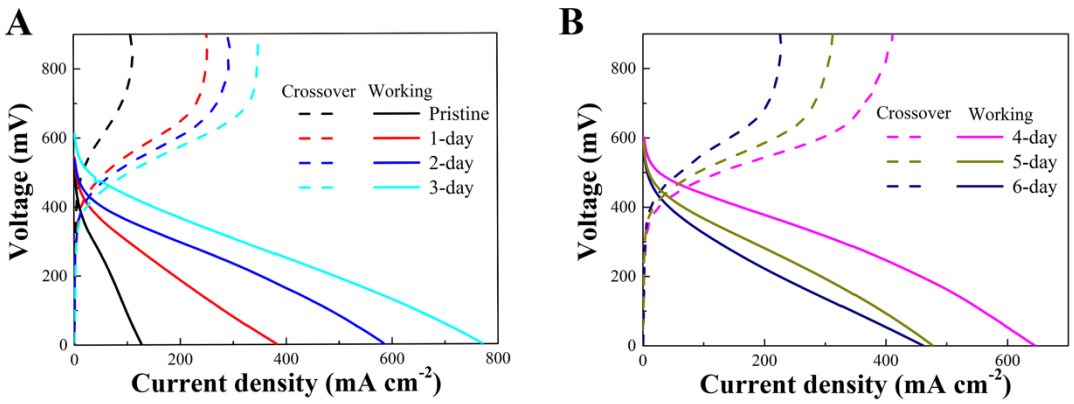

Fig. S32 Methanol crossover current *vs.* working current under 60 °C with 1 M methanol/water passing through the anode. **(A)** Pristine to 3-day treatment. **(B)** 4 to 6 days treatment.

Table S4: Maximum power density of samples with different SBD treatment time under 5 M methanol and operating temperatures ranging from 20 °C (room temperature, rt) to 70 °C. Δ is the standard deviation**.**

Treatment time (day)	Max. P (mW cm^{-2}), rt	Δ (mW cm^{-2})	Max. P (mW cm^{-2}), 40 °C	Δ (mW cm^{-2})	Max. P (mW cm^{-2}) ,50 °C	Δ (mW cm^{-2})	Max. P (mW cm^{-2}), 60 °C	Δ (mW cm^{-2})	Max. P (mW cm^{-2}) , 70 °C	Δ (mW cm^{-2})
0	8.0	0.2	13.7	4.2	22.2	9.6	25.8	15.4	17.0	0.8
1	17.4	4.7	31.8	3.7	37.4	3.3	42.9	4.6	49.7	13.2
2	21.1	1.3	38.9	2.7	48.8	8.7	60.9	10.4	70.9	17.4
3	27.8	6.8	54.9	7.7	74.2	9.5	94.4	11.2	111.4	15.9
4	38.2	5.3	66.5	4.2	89.7	4.7	109.8	14.8	133.0	17.5
5	28.0	6.3	46.6	12.3	55.7	16.1	61.3	23.1	64.4	31.6
6	22.0	7.3	37.1	14.2	45.3	18.4	44.9	17.3	45.2	21.2

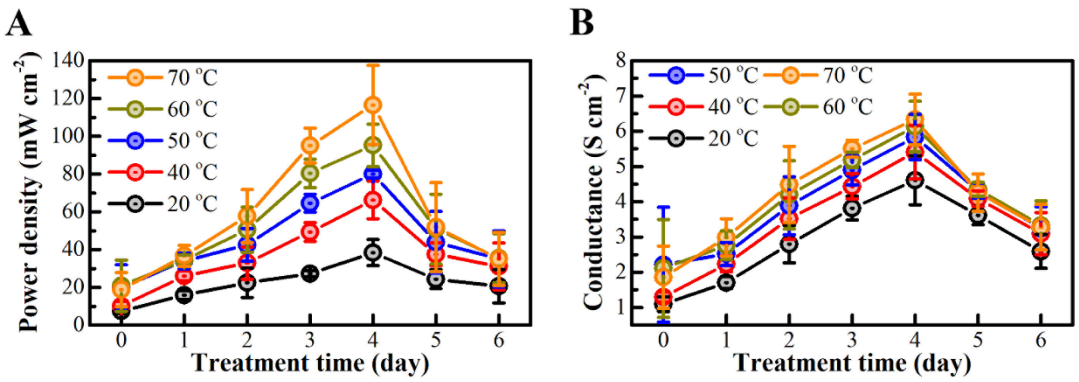

Fig. S33 Maximum power density **(A)** and conductance **(B)** of samples with different treatment time obtained, measured in DMFCs with 5 M methanol.

References.

1 te Velde, G. & Baerends, E. J. Precise density-functional method for periodic structures. *Physical Review B* **44**, 7888-7903 (1991). https://doi.org/10.1103/PhysRevB.44.7888

2 BAND 2021, SCM, Theoretical Chemistry, Vrije Universiteit, Amsterdam, The Netherlands *http://www.scm.com*

3 An, Y., Oliveira, A. F., Brumme, T., Kuc, A. & Heine, T. Stone-Wales defects cause high proton permeability and isotope selectivity of single-layer graphene. *Adv. Mater.* **32**, 2002442 (2020). https://doi.org/10.1002/adma.202002442

4 van Duin, A. C. T., Dasgupta, S., Lorant, F. & Goddard, W. A. ReaxFF: A reactive force field for hydrocarbons. *J. Phys. Chem. A* **105**, 9396-9409 (2001). https://doi.org/10.1021/jp004368u

5 Chenoweth, K., van Duin, A. C. T. & Goddard, W. A. ReaxFF reactive force field for molecular dynamics simulations of hydrocarbon oxidation. *J. Phys. Chem. A* **112**, 1040-1053 (2008). https://doi.org/10.1021/jp709896w

6 Duin, A. C. T. v. *et al.* ReaxFF 2022.1, SCM, Theoretical Chemistry, Vrije Universiteit, Amsterdam, The Netherlands. *http://www.scm.com*

7 Baerends, E. J. *et al.* ADF 2021.1, SCM, Theoretical Chemistry, Vrije Universiteit, Amsterdam, The Netherlands. *http://www.scm.com*

8 te Velde, G. *et al.* Chemistry with ADF. *Journal of Computational Chemistry* **22**, 931-967 (2001). https://doi.org/https://doi.org/10.1002/jcc.1056

9 Rahnamoun, A. & van Duin, A. C. T. Reactive Molecular Dynamics Simulation on the Disintegration of Kapton, POSS Polyimide, Amorphous Silica, and Teflon during Atomic Oxygen Impact Using the Reaxff Reactive Force-Field Method. *J. Phys. Chem. A* **118**, 2780-2787 (2014). https://doi.org/10.1021/jp4121029

10 Ganeshan, K. *et al.* Structure and dynamics of aqueous electrolytes confined in 2D-TiO2/Ti3C2T2 MXene heterostructures. *ACS Appl. Mater. Interfaces* **12**, 58378-58389 (2020). https://doi.org/10.1021/acsami.0c17536

11 Fortunato, J., Shin, Y. K., Spencer, M. A., van Duin, A. C. T. & Augustyn, V. Choice of Electrolyte Impacts the Selectivity of Proton-Coupled Electrochemical Reactions on Hydrogen Titanate. *The Journal of Physical Chemistry C* **127**, 11810-11821 (2023). https://doi.org/10.1021/acs.jpcc.3c01057

12 Senftle, T. P. *et al.* The ReaxFF reactive force-field: development, applications and future directions. *npj Comput. Mater.* **2**, 14 (2016). https://doi.org/10.1038/npjcompumats.2015.11

13 Laio, A. & Parrinello, M. Escaping free-energy minima. *Proc. Natl. Acad. Sci. U. S. A.* **99**, 12562-12566 (2002). https://doi.org/10.1073/pnas.202427399

14 Laio, A. & Gervasio, F. L. Metadynamics: a method to simulate rare events and reconstruct the free energy in biophysics, chemistry and material science. *Rep. Prog. Phys.* **71**, 22 (2008). https://doi.org/10.1088/0034-4885/71/12/126601

15 Bonomi, M. *et al.* PLUMED: A portable plugin for free-energy calculations with molecular dynamics. *Comput. Phys. Commun.* **180**, 1961-1972 (2009). https://doi.org/10.1016/j.cpc.2009.05.011

16 Barducci, A., Bussi, G. & Parrinello, M. Well-tempered metadynamics: A smoothly converging and tunable free-energy method. *Physical Review Letters* **100**, 4 (2008). https://doi.org/10.1103/PhysRevLett.100.020603

17 Park, J. M., Laio, A., Iannuzzi, M. & Parrinello, M. Dissociation mechanism of acetic acid in water. *Journal of the American Chemical Society* **128**, 11318-11319 (2006). https://doi.org/10.1021/ja060454h

18 Sun, L. Z. *et al.* Toward epitaxial growth of misorientation-free graphene on Cu(111) foils. *ACS Nano* **16**, 285-294 (2022). https://doi.org/10.1021/acsnano.1c06285

19 Li, Y. *et al.* Large Single-Crystal Cu Foils with High-Index Facets by Strain-Engineered Anomalous Grain Growth. *Adv. Mater.* **32**, 2002034 (2020). https://doi.org/https://doi.org/10.1002/adma.202002034

20 Nguyen, V. L. *et al.* Seamless Stitching of Graphene Domains on Polished Copper (111) Foil. *Advanced Materials* **27**, 1376-+ (2015). https://doi.org/10.1002/adma.201404541

21 Deng, B. *et al.* Wrinkle-Free Single-Crystal Graphene Wafer Grown on Strain-Engineered Substrates. *Acs Nano* **11**, 12337-12345 (2017). https://doi.org/10.1021/acsnano.7b06196

22 Li, X. S. *et al.* Large-Area Synthesis of High-Quality and Uniform Graphene Films on Copper Foils. *Science* **324**, 1312-1314 (2009). https://doi.org/10.1126/science.1171245

23 Barin, G. B. *et al.* Optimized graphene transfer: Influence of polymethylmethacrylate (PMMA) layer concentration and baking time on graphene final performance. *Carbon* **84**, 82-90 (2015). https://doi.org/10.1016/j.carbon.2014.11.040

24 Wang, Q. H. *et al.* Understanding and controlling the substrate effect on graphene electron-transfer chemistry via reactivity imprint lithography. *Nature Chemistry* **4**, 724-732 (2012). https://doi.org/10.1038/nchem.1421

25 Koehler, F. M., Jacobsen, A., Ensslin, K., Stampfer, C. & Stark, W. J. Selective Chemical Modification of Graphene Surfaces: Distinction Between Single- and Bilayer Graphene. *Small* **6**, 1125-1130 (2010). https://doi.org/10.1002/smll.200902370

26 Lucchese, M. M. *et al.* Quantifying ion-induced defects and Raman relaxation length in graphene. *Carbon* **48**, 1592-1597 (2010). https://doi.org/10.1016/j.carbon.2009.12.057

27 Min, H. *et al.* Ambient-ageing processes in amine self-assembled monolayers on microarray slides as studied by ToF-SIMS with principal component analysis, XPS, and NEXAFS spectroscopy. *Analytical and Bioanalytical Chemistry* **403**, 613-623 (2012). https://doi.org/10.1007/s00216-012-5862-5

28 Fairley, N. *et al.* Systematic and collaborative approach to problem solving using X-ray photoelectron spectroscopy. *Applied Surface Science Advances* **5**, 9 (2021). https://doi.org/10.1016/j.apsadv.2021.100112

29 Biesinger, M. C. Accessing the robustness of adventitious carbon for charge referencing (correction) purposes in XPS analysis: Insights from a multi-user facility data review. *Applied Surface Science* **597**, 11 (2022). https://doi.org/10.1016/j.apsusc.2022.153681

30 Hai, L. V. *et al.* Simultaneous Electroreduction of Different Diazonium Salts for Direct Electrochemical DNA Biosensor Development. *Electrochimica Acta* **140**, 49-58 (2014). https://doi.org/10.1016/j.electacta.2014.01.159

31 Fleutot, S., Dupin, J. C., Renaudin, G. & Martinez, H. Intercalation and grafting of benzene derivatives into zinc-aluminum and copper-chromium layered double hydroxide hosts: an XPS monitoring study. *Physical Chemistry Chemical Physics* **13**, 17564-17578 (2011). https://doi.org/10.1039/c1cp20453j

32 Xu, C. & Zhao, T. S. In situ measurements of water crossover through the membrane for direct methanol fuel cells. *Journal of Power Sources* **168**, 143-153 (2007).

https://doi.org/10.1016/j.jpowsour.2007.03.023

33 Seo, S. H. & Lee, C. S. A study on the overall efficiency of direct methanol fuel cell by methanol crossover current. *Applied Energy* **87**, 2597-2604 (2010). https://doi.org/10.1016/j.apenergy.2010.01.018

34 Ren, X., Springer, T. E. & Gottesfeld, S. Water and methanol uptakes in nafion membranes and membrane effects on direct methanol cell performance. *Journal of the Electrochemical Society* **147**, 92-98 (2000). https://doi.org/10.1149/1.1393161

35 Arico, A. S., Srinivasan, S. & Antonucci, V. DMFCs: From Fundamental Aspects to Technology Development. *Fuel Cells* **1**, 133-161 (2001). https://doi.org/https://doi.org/10.1002/1615-6854(200107)1:2<133::AID-FUCE133>3.0.CO;2-5